The drivers and health risks of the unexpected surface ozone enhancements over the Sichuan basin, China in 2020

Youwen Sun[1, 2], Hao Yin[1, 2,†], Xiao Lu[3,†], Justus Notholt[4], Mathias Palm[4], Cheng Liu[2], Yuan Tian[5], and Bo Zheng[6]

[1]*Key Laboratory of Environmental Optics and Technology, Anhui Institute of Optics and Fine Mechanics, HFIPS, Chinese Academy of Sciences, Hefei 230031, China*
[2]*Key Laboratory of Precision Scientific Instrumentation of Anhui Higher Education Institutes, University of Science and Technology of China, Hefei, 230026, China*
[3]*School of Atmospheric Sciences, Sun Yat-sen University, Zhuhai, 519082, China*
[4]*University of Bremen, Institute of Environmental Physics, P. O. Box 330440, 28334 Bremen, Germany*
[5]*Institutes of Physical Science and Information Technology, Anhui University, Hefei 230601, China*
[6]*Institute of Environment and Ecology, Tsinghua Shenzhen International Graduate School, Tsinghua University, Shenzhen 518055, China*
[†]Corresponding authors.
E-mail addresses: Hao Yin (yhyh95@mail.ustc.edu.cn) and Xiao Lu (luxiao25@mail.sysu.edu.cn)

Abstract

After a continuous increase in surface ozone (O_3) level from 2013 to 2019, the overall summertime O_3 concentrations across China showed a significant reduction in 2020. In contrast to this overall reduction in surface O_3 across China, unexpected surface O_3 enhancements of 10.2 ± 0.8 ppbv (23.4%) were observed in May-June 2020 vs. 2019 over the Sichuan basin (SCB), China. In this study, we use high resolution nested-grid GEOS-Chem simulation, the eXtreme Gradient Boosting (XGBoost) machine learning method, and the exposure−response relationship to determine the drivers and evaluate the health risks of the unexpected surface O_3 enhancements. We first use the XGBoost machine learning method to correct the GEOS-Chem model-to-measurement O_3 discrepancy over the SCB. The relative contributions of meteorology and anthropogenic emissions changes to the unexpected surface O_3 enhancements are then quantified with the combination of GEOS-Chem and XGBoost models. In order to assess the health risks caused by the unexpected O_3 enhancements over the SCB, total premature death mortalities are estimated. The results show that changes in anthropogenic emissions caused 0.9 ± 0.1 ppbv of O_3 reduction and changes in meteorology caused 11.1 ± 0.7 ppbv of O_3 increase in May-June 2020 vs. 2019. The meteorology-induced surface O_3 increase is mainly attributed to an increase in temperature and the decreases in precipitation, specific humidity and cloud fractions over the SCB and surrounding regions in May-June 2020 vs. 2019. These changes in meteorology combined with the complex basin effect enhance biogenic emissions of volatile organic compounds (VOCs) and nitrogen oxides (NO_x), speed up O_3 chemical production, and inhabit the ventilation of O_3 and its precursors, and therefore account for the surface O_3 enhancements over the SCB. The total premature mortality due to the unexpected surface O_3 enhancements over the SCB has increased by 89.8% in May-June 2020 vs. 2019.

Keywords: Ozone; Health risk; Emissions; Meteorology; Chemical model; Machine learning

1. Introduction

Surface ozone (O_3) is largely generated from its local anthropogenic (fossil fuel and biofuel combustions) and natural (biomass burning (BB), lightning, and biogenic emissions) precursors such as volatile organic compounds (VOCs), nitrogen oxides (NO_x), and carbon monoxide (CO) via a chain of photochemical reactions (Cooper, 2019;Sun et al., 2018). Additional portion of surface O_3 is transported from long-distance regions or from stratosphere (Akimoto et al., 2015;Wang et al., 2020b). Surface O_3 is one of the most harmful air pollutants that threatens human health and corps production (Fleming et al., 2018;Lu et al., 2020;Sun et al., 2018;Van Dingenen et al., 2009). Exposure to ambient O_3 pollution evokes a series of health risks including stroke, respiratory disease (RD), hypertension, cardiovascular disease (CVD), and chronic obstructive pulmonary disease (COPD) (Brauer et al., 2016;Lelieveld et al., 2013;Li et al., 2015;Liu et al., 2018;Lu et al., 2020;Wang et al., 2020c). Lu et al., 2020 estimated that the premature RD mortalities attributable to ambient O_3 exposure in 69 Chinese cities in 2019 reached up to 64,370.

Surface O_3 variability is sensitive to both emissions and meteorological changes (Liu and Wang, 2020a, b;Lu et al., 2019c). Meteorological conditions affect surface O_3 variability indirectly through changes in natural emissions of its precursors or directly via changes in wet and dry removal, dilution, chemical reaction rates, and transport flux (Li et al., 2019a;Lin et al., 2008;Liu and Wang, 2020a;Lu et al., 2019d). A reduction in temperature can lessen O_3 production by slowing down the chemical reaction rates (Fu et al., 2015;Lee et al., 2014;Liu and Wang, 2020a) or reducing the biogenic VOCs and NO_x emissions (Guenther et al., 2006;Im et al., 2011;Tarvainen et al., 2005). A dryer meteorological condition can result in an increase in surface O_3 level (He et al., 2017;Kalabokas et al., 2015;Liu and Wang, 2020a). Depending on which process dominates the influence of planetary boundary layer height (PBLH) on surface pollutants, a higher PBLH can either reduce surface O_3 level by diluting O_3 and its precursors into a larger volume of air (Sanchez-Ccoyllo et al., 2006;Wang et al., 2020d) or increase surface O_3 level by transporting more O_3 from upper troposphere or lessening NO abundance for O_3 titration (He et al., 2017;Liu and Wang, 2020a;Sun et al., 2009). Precipitation has been verified to decrease surface O_3 level through the wet removal of its precursors, and clouds reduce surface O_3 level by decreasing the oxidative capacity of the atmosphere and enhancing scavenging of atmospheric oxidants (Lelieveld and Crutzen, 1990;Liu and Wang, 2020b;Shan et al., 2008;Steinfeld, 1998). A higher wind speed can decrease surface O_3 level by a fast ventilation of O_3 and its precursors (Lu et al., 2019c;Sanchez-Ccoyllo et al., 2006).

Emissions of air pollutants affect surface O_3 variability by perturbing the abundances of hydroperoxyl (HO_2) and alkylperoxyl (RO_2) radicals which are the key atmospheric constituents in formation of O_3 (Liu and Wang, 2020b). Many previous studies have verified a nonlinear relationship between O_3 and its precursors (e.g., (Atkinson, 2000;Liu and Wang, 2020b;Lu et al., 2019d;Sun et al., 2018;Wang et al., 2017). If surface O_3 formation regime lies within the VOCs limited region, reductions in VOCs emissions will result in a reduction in surface O_3 level. Similarly, if surface O_3 formation regime lies within the NO_x limited region, reductions in NO_x emissions will result in a reduction in surface O_3 level (Atkinson, 2000;Wang et al., 2017). If surface O_3 formation regime lies within transitional region, reductions in either VOC or NO_x emissions will result in a

reduction in surface O_3 level. Atmospheric aerosols can affect surface O_3 level through either heterogeneous reactions of reactive gases (Li et al., 2018;Lou et al., 2014;Lu et al., 2012;Stadtler et al., 2018) or affecting the solar radiation for gases photolysis and oxidation (Li et al., 2011;Lu et al., 2019c;Lu et al., 2019d;Xing et al., 2017).

Understanding the drivers of surface O_3 variability has a strong implication for O_3 mitigation purpose (Chen et al., 2020;Lu et al., 2019c;Sun et al., 2018). China has experienced a continuous increase in surface O_3 level despite the implementation of control measures on NO_x since 2013 (Liu and Wang, 2020a, b;Lu et al., 2018;Lu et al., 2020). Many studies have attempted to determine the drivers of high-O_3 events occurred in specific region and time across China. Most of these studies focus on the most densely populated and highly industrialized areas in eastern China, whereas the studies in the rest part of China are still limited (Liu and Wang, 2020a, b;Lu et al., 2019a;Lu et al., 2019b;Lu et al., 2012;Wang et al., 2020a;Wang and Lu, 2019;Wang et al., 2017). As China has a vast territory with a wide range of emission levels and meteorological conditions, O_3 variability and its drivers may vary both temporally and geographically, so the results from one region are not likely to be applied nationally. In addition, previous studies typically use state-of-the-art chemical transport models (CTMs) with sensitivity simulations to quantify the drivers of O_3 variability, e.g., fixed meteorology but varied emission levels to quantify the influences of emission changes or vice versa (Liu and Wang, 2020a, b;Lu et al., 2019a). However, uncertainties in local meteorological fields, emission estimates, and model mechanisms can lead to a discrepancy in CTMs that may affect the accuracy of O_3 predictions and their sensitivities to changes in emissions and meteorology (Lu et al., 2019c;Young et al., 2018). This is in particular for the Sichuan basin (SCB), one of the most industrialized and populated cities cluster in western China, where large discrepancies between measured and modelled surface O_3 are found due to the complex terrain (Lu et al., 2019c;Wang et al., 2020d).

After a continuous increase in surface O_3 level from 2013 to 2019, the summertime (May-August) O_3 concentration across China showed a significant reduction in 2020 (Figure 1 (d)). In this study, we use high resolution nested-grid GEOS-Chem simulation, the eXtreme Gradient Boosting (XGBoost) machine learning method, and the exposure−response relationship to determine the drivers and evaluate the health risks of the unexpected surface O_3 enhancements. We first use the XGBoost machine learning method to correct the GEOS-Chem model-to-measurement O_3 discrepancy over the SCB. The relative contributions of meteorology and anthropogenic emissions changes to the unexpected surface O_3 enhancements are then quantified with the combination of GEOS-Chem and XGBoost models. In order to assess the health risks caused by the unexpected O_3 enhancements over the SCB, total premature death mortalities are also estimated.

2. Methods and data

2.1 Surface O_3 data and auxiliary data over the SCB

China has identified nine city clusters that lead the populations and developments of economy, society, and culture across China. The SCB contains the fourth-largest cities cluster in China after the Yangtze River Delta (YRD), the Pearl River Delta (PRD), and the Beijing-Tianjin-Hebei (BTH) cities clusters. The location of the SCB city cluster is shown in Figure S1. With Chongqing and Chengdu as the dual core cities, more than a dozen cities including Mianyang, Deyang, Yibin, Nanchong, Dazhou, and Luzhou over the SCB have achieved rapid economic development and

industrial upgrading. As the region with the strongest economic strength and best economic foundation in western China, the SCB region has many industries such as energy and chemical industry, electronic information, food processing, equipment manufacturing, eco-tourism, and modern finance. As one of the most densely populated and highly industrialized regions in China combined with the basin terrain which is favorable to the accumulation of air pollutants, the SCB is a newly emerging region of severe air pollution in China (Lu et al., 2019b;Lu et al., 2012).

Surface O_3 measurements over the SCB are available from the China National Environmental Monitoring Center (CNEMC) network (http://www.cnemc.cn/en/, last access: 2 July 2021). The CNEMC network has routinely measured the concentrations of CO, O_3, NO_2, SO_2, PM_{10}, and $PM_{2.5}$ at 122 sites in 22 key cities over the SCB since 2015. The mean geolocation, population, the number of measurement site, and data range of each city are summarized in Table 1. The altitude of these cities ranges from 0.3 to 4.3 km (above sea level, a.s.l.) and the population ranges from 822 to 32,054 thousand. The number of measurement site in each city ranges from 2 to 21. Surface O_3 measurements at all measurement sites are based on similar differential absorption ultraviolet (UV) analyzers. The hourly mean time series of surface O_3 concentrations have covered the period from January 2015 to present at all measurement sites in the 22 cities. After removing unreliable measurements with the filter criteria used in (Lu et al., 2020) (Section S1), we average the O_3 concentrations at all measurement sites in each city to form a city representative O_3 dataset. O_3 metric used in this study is on maximum 8-h average (MDA8) basis.

Since the vertical distributions of tropospheric HCHO and NO_2 are weighted heavily toward the lower troposphere over polluted regions, many studies have used tropospheric column measurements of these gases to represent near-ground conditions (Streets et al., 2013;Sun et al., 2021b;Sun et al., 2018). In this study, the tropospheric NO_2 and HCHO columns from the TROPOMI Level 3 products are used for investigating the changes in O_3 precursors in May-June 2020 vs. 2019. TROPOMI overpasses China at approximately 13:30 local time (LT) with a ground pixel size of 7 km × 7 km. Pixels with quality assurance values of less than 50% for HCHO and 75% for NO_2 are not included in present work.

2.2 GEOS-Chem nested-grid simulation

We use the high resolution nested-grid GEOS-Chem model version 12.2.1 to simulate surface O_3 over the SCB (Bey et al., 2001). Simulations are conducted at a horizontal resolution of 0.25 °× 0.3125 ° over the nested domain (70 °-140 °E, 15 °-55 °N) covering China and surrounding regions. The boundary conditions for the nested-grid GEOS-Chem simulation are archived from the global simulation at 2 °× 2.5 ° resolution (Sun et al., 2021a;Sun et al., 2021b;Yin et al., 2020;Yin et al., 2019) We spun up the model for one year to remove the influence of the initial conditions. We first run global simulation at 2 °× 2.5 °resolution and then interpolate the restart file on 1 January 2018 into high resolution (0.25 °× 0.3125 °) for the nested domain to initialize the nested model simulation from January 2019 to June 2020.

The simulations were driven by GEOS-FP meteorological field at the native resolution of 0.25° × 0.3125° and 47 layers from surface to 0.01 hPa at the top. The PBLH and surface meteorological variables are implemented in 1-hour interval and other meteorological variables are in 3-hour intervals. The time step applied in the model for transport is 5 minutes and for chemistry and emissions is 10 minutes (Philip et al., 2016) The non-local scheme for the boundary layer mixing

process is from (Lin and McElroy, 2010), wet deposition is from (Liu et al., 2001), and dry deposition is generated with the resistance-in-series algorithm (Wesely, 1989;Zhang et al., 2001). The photolysis rates are from the FAST-JX v7.0 photolysis scheme (Bian and Prather, 2002). Chemical mechanism follows the universal tropospheric-stratospheric Chemistry (UCX) mechanism (Eastham et al., 2014). The GEOS-Chem simulation outputs 47 layers of O_3 and other atmospheric constituents over China with a temporal resolution of 1 hour.

We use the Community Emissions Data System (CEDS) inventory for global anthropogenic emissions at the latest 2017 level, which is overwritten by the Chinese anthropogenic emissions with the Multi-resolution Emission Inventory (MEIC) in 2019 (Hoesly et al., 2018;Li et al., 2017;McDuffie et al., 2020;Zheng et al., 2018). Anthropogenic emissions are fixed for 2019 and 2020. Global BB and biogenic emissions were from the Global Fire Emissions Database (GFED v4) inventory (Giglio et al., 2013) and the Model of Emissions of Gases and Aerosols from Nature (MEGAN version 2.1) inventory (Guenther et al., 2012), respectively. Soil NO_x emissions (Hudman et al., 2010;Lu et al., 2021) and lightning NO_x (Murray et al., 2012) emissions are calculated online in the model.

2.3 Correction of GEOS-Chem discrepancy with machine learning method

We used the XGBoost machine learning method to correct the GEOS-Chem model-to-measurement O_3 discrepancy over the SCB following (Keller et al., 2021). The same methodology has also been applied in our companion study examining ozone changes over the eastern China from 2019 to 2020 (Yin et al., 2021). It uses the Gradient Boosting Decision Tree (GBDT) framework to iteratively train the GEOS-Chem model-to-measurement discrepancy to improve the model predictions in a stagewise manner. XGBoost method minimizes the loss function by adding a weak learner for the purpose of optimizing the objective function. The optimization objective function used in XGBoost model is expressed as,

$$L^{(t)} \simeq \sum_{i=1}^{n}[l(y_i, \hat{y}^{(t-1)}) + g_i f_t(x_i) + \frac{1}{2} h_i f_t^2(x_i)] + \Omega(f_t) \quad (1)$$

$$g_i = \partial_{\hat{y}^{(t-1)}} l(y_i, \hat{y}^{(t-1)}) \quad (2)$$

$$h_i = \partial^2_{\hat{y}^{(t-1)}} l(y_i, \hat{y}^{(t-1)}) \quad (3)$$

where g_i and h_i are first and second order gradients of the loss function, respectively. $L^{(t)}$ represents the optimization objective function to be solved at the t-th iteration. $l(y_i, \hat{y}^{(t-1)})$ is the loss function representing the difference between the prediction for the i-th sample at the (t-1)-th iteration and the real values y_i. Function $f(t)$ is the amount of change at the t-th iteration. Overall, the objective function consists of a two-order Taylor approximation expansion of the loss function and the regularization term ($\Omega(f_t)$), which penalizes the complexity of the model and prevents overfitting of the model. Compared to traditional GBDT method, XGBoost method has the following advantages: (1) effectively handles missing values; (2) prevents overfitting; (3) reduces computing time by using parallel and distributed computing methods.

Since GEOS-Chem model-to-measurement discrepancy is usually site-specific, we train a separate XGBoost model for each site. Similar to the method of (Keller et al., 2021), we use a full seasonal cycle of hourly measurements in 2019 at each site as the learning samples, and GEOS-

Chem input of emissions and meteorological parameters, output concentrations of atmospheric constituents, and time information as training input data. In order to incorporate emissions and meteorological factors that affect O_3 production properly, we have included the GEOS-Chem simulated concentrations of 43 atmospheric chemical constituents, emissions of 21 atmospheric chemical constituents, 10 meteorological parameters, and 4-time parameters (e.g., hour, day, month, and year) into the data training. All these training input data are summarized in Table S1 and have been standardized as equation (2) in section S2. We choose a learning rate of 0.35, maximum tree depth of 6, L1 and L2 regularization terms of 0 and 1, the loss function of mean square, and evaluation metric of root-mean-square error (RMSE) in the data training.

We use *k*-fold cross-validation method to test the performance of the XGBoost model (*k*=1 – *n*). First, all sample data are randomly and uniformly divided into *k* groups, where one group is taken as the test dataset and the remaining *k*-1 groups are taken as the training dataset. We then start to train the model and use the test dataset to evaluate the performance of the trained model. We repeated this process for *k* times by using different groups of datasets as the test data. The training model is finally determined if all the *k* groups of experiments show similar performances. This method ensures the stability and robustness of XGBoost model and avoid overfitting. In this study, a 10-fold cross-validation method is applied, i.e., we divide the O_3 measurements in 2019 into 10 groups of sub data: the training dataset accounts for 90% and the test dataset accounts for the remaining 10% of the total sample data. We also attempted to use 60% and 80% of the sample data as the training dataset and do not find significant influences on the results, indicating the robustness of the XGBoost training model.

2.4 Quantifying meteorological and emissions contributions

We have used the GEOS-Chem only and the combination of GEOS-Chem and XGBoost model (hereafter GEOS-Chem-XGBoost) to quantify the contributions of meteorology and anthropogenic emissions to the unexpected surface O_3 enhancements over the SCB in 2020, following (Yin et al., 2021). For the GEOS-Chem method, since the anthropogenic emissions are fixed, the simulated O_3 differences between 2020 and 2019 can be attributed to changes in meteorological conditions, which is calculated as,

$$G\_Met = G_{2020} - G_{2019} \quad (4)$$

The contribution of anthropogenic emissions changes can then be quantified as,

$$G\_Emis = (Meas_{2020} - Meas_{2019}) - G\_Met \quad (5)$$

where *G_Met* and *G_Emis* represent the meteorology and anthropogenic emissions contributions, respectively. $Meas_{2019}$ and $Meas_{2020}$ represent O_3 measurements in 2019 and 2020, respectively. G_{2019} and G_{2020} represent GEOS-Chem O_3 simulations in 2019 and 2020, respectively.

Since the GEOS-Chem-XGBoost model has corrected the GEOS-Chem model-to-measurement discrepancy in 2019, we assume it can provide accurate predictions to the surface O_3 measurements in 2020 if the anthropogenic emissions were unchanged. This assumption is valid since the probability density functions (PDFs) of key O_3 precursors and meteorological parameters for the training data within a full seasonal cycle of 2019 cover the variation ranges of these factors in May-June 2020 (Figures S2 and S3). For predicting O_3 evolutions in 2020, all input parameters except anthropogenic emissions fed into each GEOS-Chem-XGBoost model are updated to match the measurements in 2020, while anthropogenic emissions are fixed at the 2019 levels. As a result,

the differences between the GEOS-Chem-XGBoost predictions for 2020 and the 2020 measurements are attributed to the changes in anthropogenic emissions (equation (6)). The meteorology induced contributions are then obtained as equation (7) by subtracting the anthropogenic emissions induced contributions.

$$XG\_Emis = Meas_{2020} - XG_{2020} \quad (6)$$

$$XG\_Met = (Meas_{2020} - Meas_{2019}) - XG\_Emis \quad (7)$$

where the acronyms are similar to those in equations (4) and (5) but for GEOS-Chem-XGBoost method. By correcting the model-to-measurement discrepancy, GEOS-Chem-XGBoost model is expected to provide a more accurate O_3 sensitivity to changes in both meteorology and anthropogenic emissions as will be discussed later.

2.5 Health risks evaluation

We have assessed the total premature mortalities including all nonaccidental causes, hypertension, CVD, RD, COPD, and stroke attributed to ambient O_3 exposure in all cities over the SCB in 2019 and 2020. We first calculated the O_3 induced daily premature mortalities based on the exposure−response relationship described in Cohen et al., 2004, which have been used in many subsequent studies (Anenberg et al., 2010;Liu et al., 2018;Wang et al., 2021). We then added up the daily premature mortalities within May-June or the whole year to get the total O_3 induced premature mortalities in the respective periods. The population data used in this study include all age groups, which may result in higher daily mortalities than expected (Liu et al., 2018;Wang et al., 2021). According to (Cohen et al., 2004), the daily premature mortalities attributable to ambient O_3 exposure can be estimated by the following equation (Cohen et al., 2004),

$$\Delta x = \begin{cases} 0, & (if \quad C_{meas} - C_{thres} \le 0) \\ C_{meas} - C_{thres}, & (if \quad C_{meas} - C_{thres} \ge 0) \end{cases} \quad (8)$$

$$\Delta M = y_0[1 - \exp(-\beta \Delta x)] \times Pop \quad (9)$$

where ΔM represents the daily premature mortalities due to ambient O_3 exposure. The city representative daily mean O_3 concentration C_{meas} is an average of all measurements in each city. Variable y_0 is the daily baseline mortality rate for each disease averaged from all ages and genders. We follow the method of (Wang et al., 2021) and use the daily y_0 value for each disease from the latest China Health Statistical Yearbook in 2018. β represents the increase in daily mortality as a result of each 10 μg/cm^3 (~ 5.1 ppbv) increase in daily O_3 concentration, which is often referred to as the concentration response function (CRF) in previous studies. We collected the CRF values from those used in (Yin et al., 2017) and (Wang et al., 2021). Δx represents the incremental O_3 concentration relative to the threshold concentration C_{thres} of 35.1 ppbv, which is obtained from (Lim et al., 2012) and (Liu et al., 2018). Pop represents the population exposed in the ambient O_3 pollution, which is available from the seventh nationwide population census in 2020 provided by National Bureau of Statistics of China. The daily y_0 and β values for all non-accidental causes, hypertension, CVD, RD, COPD, and stroke are summarized in Table S2.

3 Unexpected surface O_3 enhancements over the SCB in 2020

Figures 1(a)-(b) show the May-June mean MDA8 O_3 concentrations at all measurement sites over the SCB in 2019 and 2020. The May-June mean MDA8 O_3 concentrations averaged over all

cities in the SCB region in 2019 and 2020 are 48.1 ppbv and 58.3 ppbv, which are 11.0 ppbv lower and 1.2 ppbv higher than those averaged over all Chinese cities in the same period, respectively. As the most densely populated and highly industrialized region in western China, the land use, industrialization, infrastructure construction, and urbanization over the SCB have expanded rapidly in recent years, resulting in the highest anthropogenic emissions of O_3 precursors and highest surface O_3 levels in the region (Figure S4). Although the O_3 levels in the SCB cities cluster are lower than those in the three most developed city clusters in eastern China, i.e., the BTH, the Fenwei Plain (FWP), and the YRD city clusters, the SCB region has been classified by the MEE as a newly pollution region for O_3 mitigation (Sun et al., 2021b;Wang et al., 2020a;Wang and Lu, 2019;Zou et al., 2019). Situated in the basin with stationary meteorological fields combined with high anthropogenic emissions, the SCB cities cluster is potential to become a new region with frequent high-O_3 events after BTH, FWP, and YRD.

We find significant O_3 enhancements by 10.2 ± 0.8 ppbv (23.4%) (mean $\pm 1\sigma$ standard deviation) averaged over all cities in the SCB in May-June 2020 vs. 2019 levels (Figure 1(c)). The largest enhancements are observed in the most densely populated areas around the megacities Chongqing and Chengdu (11.8 ± 0.6 ppbv (29.9%)). These year-to-year O_3 enhancements over the SCB are record high in the 2015-2020 period, following an increasing change rate of 1.2% yr^{-1} from 2015 to 2017 and then a decreasing change rate of −0.7% yr^{-1} from 2017 to 2019. These surface O_3 enhancements mainly reflect regional emissions and meteorology changes in the SCB and surrounding regions since the lifetimes of surface O_3 and most of its precursors are too short to undergo long range transport.

The significant O_3 enhancements over the SCB in May-June 2020 vs. 2019 are opposite to the overall decrease in surface O_3 levels across China in the same period (Figure 1 (d)). After a continuous increase in surface O_3 levels from 2013 to 2019 by approximately 5% yr^{-1} (Figure 1(d)), the MDA8 O_3 averaged over all cities outside the SCB across China in May-June 2020 vs. 2019 levels showed a significant reduction of 5.3 ± 0.5 ppbv (8.3%). Such O_3 reductions are widespread in the eastern China, especially in the BTH, FWP, and YRD regions, and we have investigated their drivers in a separate study (Yin et al., 2021).

4 Model performance assessment

We use the metrics of normalized root-mean-square error (NRMSE), normalized mean bias (NMB), and Pearson correlation coefficient (R) to assess the performance of the GEOS-Chem-XGBoost model. For each measurement site, we analysed these metrics for both training (blue) and test (red) datasets as shown in Figure S5. We define the NRMSE as the RMSE normalized by the difference between the 95th and 5th percentile concentrations, and NMB as the mean bias normalized by average concentration at the given measurement site. The formulas of above metrics are summarized in Section S2.

The GEOS-Chem-XGBoost model predictions for surface O_3 over the SCB show no bias when evaluated against the training data, with NMB of 0.01, NRMSEs of less than 0.1, and R between 0.93 – 1.0. Compared to the training data, the performances on the test data show a higher variability, with an average NMB of –0.04, NRMSE of 0.22, and R of 0.83. We find no significant difference in prediction performance between clean (less than the C_{thres} defined in section 2.5) and polluted measurement sites. A number of factors likely contribute to relatively poorer statistical results at

some sites such as Ganzizhou, Leshan, and Suining. First, the training data of these sites may include certain temporal events that are not easily generalizable, such as unusual emissions activity (e.g., BB, fireworks, closure of nearby point source) or weather patterns that are not properly observed, which might be prone to overfitting. In addition, the differences in surface O_3 variabilities between the training data and the test data at these sites are relative larger than other sites, which can contribute to a relative poorer performance.

We use the SHapely Additive exPlanations (SHAP) approach to examine how the GEOS-Chem-XGBoost model uses the input variables to make a prediction. The SHAP approach is based on game-theoretic Shapely values and represents a measure of each predictor's responsibility for a change in the model prediction (Lundberg and Lee, 2017). The SHAP values are computed separately for each model prediction, which offer detailed insight into the importance of each input variable to this prediction while also consider the role of variables interactions (Keller et al., 2021;Lundberg et al., 2020). Figure 2 shows the SHAP value distribution for all the major O_3 predictors averaged over all cities in the SCB. The results show that all variables that are expected to be associated with O_3 formation can affect model O_3 prediction. Generally, the temperatures (at the surface, 2 m height, and 10 m height) are the most important predictors for the GEOS-Chem model-to-measurement discrepancy over the SCB, followed by the uncorrected GEOS-Chem simulated O_3, reactive nitrogen (e.g., NO_2, Peroxyacetyl nitrate (PAN)), atmospheric oxidants (O_x, hydrogen peroxide (H_2O_2)), fine aerosols, VOCs (Isoprene, C_3H_8), hour of the day, and meteorological variables including horizontal and vertical wind speeds (u10m, v10m). All of these factors have tight connections to surface O_3 formation over the SCB and it is thus not surprising that the GEOS-Chem model-to-measurement discrepancies are most sensitive to them (Seinfeld and Pandis, 2016).

We have compared the performances of GEOS-Chem and GEOS-Chem-XGBoost in capturing the measured surface O_3 levels. Figure 3 (a) shows the time series of measured and model predicted O_3 concentrations averaged over all cities in the SCB region. Figure 3 (b) shows histogram of the differences between the GEOS-Chem-XGBoost predictions and the measurements. The GEOS-Chem simulations generally capture the daily variability of MDA8 O_3 over the SCB, but they show a high bias of 7.8 ± 5.0 ppbv (17.5%) across all measurement sites within the SCB region. The discrepancy can be mainly attributed to uncertainties in the horizontal transport and vertical mixing schemes simulated by the GEOS-Chem model at a relatively coarse spatial resolution compared to the measurements at a single point, and also associated with the errors in emission estimates, chemical mechanism, and the sub-grid-scale local meteorological processes. Especially, errors of O_3 predictors with high SHAP values are more likely to result in large model-to- measurement discrepancy. For example, GEOS-Chem model overestimates the correlations between surface O_3 concentration and temperature (Figure S7 (a)), indicating that this overestimation of O_3-to-temperature sensitivity is one of the major factors contributing to higher GEOS-Chem model O_3 predictions.

By iteratively training and correcting the GEOS-Chem model-to-measurement discrepancy in O_3-to-temperature sensitivity, the correlations between temperature and surface O_3 concentration predicted by the GEOS-Chem-XGBoost model were in good agreement with the measurements (Figure S7 (a)). With respect to the performance of reproducing the sensitivities of O_3 to other meteorological parameters such as humidity, cloud fraction, and precipitation, the GEOS-Chem-XGBoost model is also better than the GEOS-Chem (Figure S7 (b)-(d)). After correcting the errors

in all O_3 predictors, the GEOS-Chem-XGBoost model significantly improves the prediction of surface O_3 concentrations in all cities over the SCB compared to the GEOS-Chem (Figure S8). It shows a bias of 0.5 ± 0.3 ppbv for all O_3 measurements in 2019 over the SCB. As a result, the overall GEOS-Chem-XGBoost model performance is acceptable and can support further investigation of the drivers of the unexpected surface O_3 enhancements over the SCB in May-June 2020.

5 Attribution

5.1 Separation of meteorological and anthropogenic emissions contributions

We quantify the surface O_3 enhancements in May-June 2020 over the SCB to changes in anthropogenic emissions and meteorological conditions according to equations (6) and (7). Differences between the measured and GEOS-Chem-XGBoost predicted O_3 in May-June 2020, as indicated by the shadings in Figure 4(a), represent the anthropogenic emissions-induced O_3 changes in 2020 vs. 2019. Mean contributions driven by changes in anthropogenic emissions and meteorological conditions are summarized in Figure 4(b). Due to the different change rates in anthropogenic emissions in May and June in 2020 (see section 5.3), the changes in anthropogenic emissions caused an overall increase in surface O_3 level in May but a reduction in surface O_3 level in June (Figure 4 (a)). For the May-June mean contributions averaged over all cities in the SCB, changes in anthropogenic emissions caused 0.9 ± 0.1 ppbv of O_3 reduction and changes in meteorology caused 11.1 ± 0.7 ppbv of O_3 increase, which correspond to –8.0% and 108% of relative contributions to the total O_3 enhancement (10.2 ± 0.8 ppbv) over the SCB in May-June 2020, respectively. As a result, the anthropogenic emissions induced O_3 reductions are dominantly overwhelmed by the meteorology induced O_3 increases, leading to the unexpected O_3 enhancements over the SCB in 2020.

We compare the meteorology and anthropogenic emissions induced contributions to the unexpected surface O_3 enhancements estimated by the GEOS-Chem-XGBoost model with those by the GEOS-Chem model only (Figure 4 (b)). Both methods show that changes in meteorology contribute significantly to the O_3 enhancements, while the absolute magnitudes differ slightly from each other. For example, the anthropogenic emissions induced O_3 reduction calculated with the GEOS-Chem model only is 0.94 ppbv, while the value for GEOS-Chem-XGBoost model is 1.36 ppbv. By taking the subtraction in equation (5) and the average over all cities, the propagation of systematic model discrepancies that are common to all measurements sites was effectively minimized, which can mitigate the difference in attribution results between the GEOS-Chem and GEOS-Chem-XGBoost methods. However, as demonstrated in Figure S8, model discrepancies may differ between regions and time. Therefore, the GEOS-Chem-XGBoost approach is expected to provide a more accurate and consistent estimate on O_3 change attribution than the GEOS-Chem model alone.

5.2 Meteorological contribution

Figure 5 shows the terrain elevations and May-June mean wind fields and surface pressures over the SCB and surrounding regions. The terrain altitudes, at a resolution of 3 × 3 arc-minute, indicate a rapid change in altitude from the Tibetan Plateau (4.0 –5.0 km) and Yunan-Kweichou Plateau (2–3 km) to the SCB (0.5 km). The SCB is located in the saddle between the Tibetan and

Yunnan-Kweichou Plateau (Chen et al., 2009;Sun et al., 2021c). Figure 5 (b) are the May-June mean wind fields at 500 m overlaid with surface pressure available from GEOS-FP fields at 0.25 °× 0.3125 ° resolution. In May-June, the Tibetan High formed over the middle region of the Tibetan Plateau with the western Pacific Subtropical High shifts westward to the west of the SCB (Chen et al., 2009). The southwesterly East Asian summer monsoon generates a cyclonic pattern over the southeast part of the SCB. Driven by large-scale circulations, southwesterly flow enters the east part of the SCB near the northwest edge of the Yunnan-Kweichou Plateau, while strong northwesterly flow enters the SCB near the east edge of the Tibetan Plateau. The interaction of these two flows results in a convergent zone of northward jet stream over the east part of the SCB due to the westward shift of the Western Pacific Subtropical High and the blocking effect of topography. Furthermore, strong instability of vertical convection could originate over the basin and move toward the east part of the SCB as dry air continuously entered the upper layer over the SCB (Chen et al., 2009). This process makes it a favorable region for trapping air pollutants within the SCB region (Chen et al., 2009;Liu et al., 2003).

Figure 6 shows the May-June mean differences in vertical velocity, precipitation, temperature, specific humidity, cloud fraction, and PBLH between 2020 and 2019. In May-June 2020, the northwest, central western and southern China experienced anomalous strong droughts (https://quotsoft.net/air/), leading to a significant increase in temperature and decreases in precipitation, specific humidity and cloud fractions compared to the 2019 levels (Figure 6). These changes in meteorological conditions could enhance the natural emissions of O_3 precursors and speed up O_3 chemical production. Meanwhile, the SCB basin effect inhabited the ventilation of O_3 and its precursors, which further enhanced the O_3 accumulations over the SCB. As a result, we conclude that the meteorological anomalies combined with the complex basin effect caused the surface O_3 enhancements over the SCB in 2020. Although higher PBLH over the SCB in May-June 2020 vs. 2019 may reduce surface O_3 levels by diluting O_3 and its precursors into a larger volume of air, this reduction effect was overwhelmed by the aforementioned enhancement effect. There is no strong evidence for the change in the horizontal transport from other regions (Figure 5(b)) and the vertical transport from the free troposphere to the surface (Figure 6 (a)) over the SCB in May-June 2020 vs. 2019 (Lefohn et al., 2012;Skerlak et al., 2014;Stohl et al., 2003;Wang et al., 2020a;Wang and Lu, 2019;Wang et al., 2020b;Wang et al., 2020c;Wirth and Egger, 1999). It is worth noting that, with similar meteorological anomalies in May-June 2020 vs. 2019, the O_3 enhancements were not observed in the northwest China such as Xinjiang and Inner Mongolia Provinces, and southern China such as the Pearl River Delta (PRD) region, which is also one of the nine well-developed city clusters in China with severe air pollution. This can be partly attributed to low anthropogenic emissions of O_3 precursors in northwest China (Zheng et al., 2018); and that strong exchange between the land and sea in the coastal regions driven by the summer monsoon facilitates the ventilation of O_3 and its precursors in the PRD region. Furthermore, the meteorology induced O_3 enhancements are probably overwhelmed by the anthropogenic emissions induced O_3 reductions in the northwest and southern China.

5.3 Emissions contribution

To suppress the spread of coronavirus pandemic 2019 (COVID-19) across China and above, the Chinese government sealed off several cities starting in January 2020; implementing a few

measures such as closing local businesses and halting public transportation at an unprecedented scale (Li et al., 2019b;Steinbrecht et al., 2021;Yin et al., 2021). These prevention measures quickly spread nationwide. Although the COVID-19 lockdowns in all cities have been removed before May, there are still restrictions on public transportation, businesses, social activities and industrial manufactures, which could cause domestic anthropogenic emissions reductions in both HCHO and NO_x. Furthermore, the MEE continues the mitigation of NO_x emissions following the 2018–2020 Action Plan on Defending the Blue Sky, and has also implemented The 2020 Action Plan on VOCs Mitigations in 2020. This new Action Plan issues a number of control measures including implementation of stringent VOCs emission standards, replacement of raw and auxiliary materials with low VOCs content, and mitigation of unorganized emissions. Driven by the above factors, the TROPOMI observed tropospheric HCHO and NO_2 over China in May-June 2020 vs. 2019 reduced by 2.0 ± 0.3% (averaged for all Chinese cities) and 1.1 ± 0.2%, respectively. Due to the relative short lifetime of both HCHO and NO_2 in troposphere, these reductions mostly reflect local emissions changes. These reductions in domestic anthropogenic emissions dominated the significant reduction of summertime MDA8 O_3 across China in 2020 vs 2019.

We have used the HCHO/NO_2 ratios following the method of (Sun et al., 2018) to investigate the O_3 production regime over the SCB region. The results show that the satellite observations of HCHO/NO_2 ratios in May-June in most cities over the SCB have indicated a shift toward high values from 2019 to 2020 but the O_3 chemical sensitivity in 2020 still lies within the transitional regime (Jin et al., 2017;Jin and Holloway, 2015; Figure S9). Meanwhile, the O_3 chemical sensitivity in May 2020 is similar to that in June, indicating that the O_3 variability in May-June 2020 is sensitive to both NO_x and VOCs. The recently available Chinese anthropogenic emissions statistic data provided by the MEE show that the anthropogenic VOCs over the SCB has decreased by 5.0% and 3.5% in May and June in 2020 relative to the 2019 level, respectively. The anthropogenic NO_x in the same period has increased by 1.5% and decreased by 1.7%, respectively (Zheng et al., 2021). The increase in anthropogenic NO_x in May 2020 vs. 2019 is attributed to an increase in NO_x emission from power plant sector, which was not affected by the post-lockdown restrictions for suppressing the spread of COVID-19 (Table S3). For the May-June aggregation, the anthropogenic VOCs and NO_x over the SCB have decreased by 4.3% and 0.3%, respectively (Zheng et al., 2021). These independent analyses on anthropogenic emissions explain the different predicted O_3 changes due to anthropogenic emissions alone in May (increase) versus June (decrease) in the SCB.

In contrast to the widespread reductions in both HCHO and NO_2 across the BTH, FWP, and YRD regions, we find notable increases in both HCHO and NO_2 in the SCB in May-June 2020 vs. 2019 levels. The tropospheric HCHO and NO_2 columns averaged over all cities in the SCB region have been increased by (2.8 ± 0.3%) and (5.1 ± 0.5%) in 2020 vs. 2019 levels, respectively. Since both anthropogenic VOCs and NO_x emissions in the SCB showed decreasing change rates in May-June 2020 vs. 2019, these regional increases in both HCHO and NO_2 could thus be attributed to natural emissions enhancements in both VOCs and NO_2 in the SCB. Indeed, natural emissions of biogenic VOCs and soil NO_x calculated online in the GEOS-Chem model show increasing change rates in May-June 2020 vs. 2019 in the SCB and surrounding regions (Figure 7). These enhanced biogenic VOCs and NO_x emissions are most likely driven by the hotter and dryer meteorological conditions in the SCB and surrounding regions (Figure 7).

Finally, we concluded that natural emissions enhancements of both NO_x and VOCs induced by the unexpected meteorological anomalies could be accounted for the O_3 enhancements in May-June

2020 over the SCB, and their contributions have been included in the meteorology-driven ozone enhancement as discussed in Section 5.2. In present work, we were not able to determine which specific VOCs species are the most effective for O_3 enhancements and cannot quantify the relative contributions of VOCs and NO_x enhancements to the O_3 enhancements in the SCB. A series of sensitivity studies might be able to address this important issue, but this is beyond the scope of present work.

6 Health risks for the O_3 enhancements over the SCB

Figure 8 presents the total premature mortalities from all non-accidental causes, hypertension, CVD, RD, COPD, and stroke attributable to ambient O_3 exposure in all cities over the SCB during May-June in 2019 and 2020. The statistical results for each city in 2019 and 2020 are summarized in Tables S4 and S5, respectively. The surface O_3 enhancements over the SCB in May-June 2020 vs. 2019 results in dramatically higher health risks. The estimated total premature mortalities from all non-accidental causes due to the surface O_3 enhancements in May-June 2020 over the SCB is 5455, which is 89.8% higher than that in the same period in 2019 (i.e., 2874). All above O_3 induced diseases over the SCB have significant increases in total mortalities in May-June 2020 vs. 2019. The highest health risk among these diseases is from CVD which is 741 in May-June 2019, followed by RD (236), COPD (231), and hypertension (223). This O_3 induced health risk rank over the SCB is consistent with those in the YRD, BTH, and PRD in previous studies (Liu et al., 2018; Lu et al., 2020; Yin et al., 2017; Wang et al., 2021). In May-June 2020, total mortalities from CVD, RD, COPD, hypertension, and stroke over the SCB reached to 1405, 450, 439, 418, and 46, respectively, due to significant O_3 enhancements. The change rates for these diseases are 89.6, 90.7, 90.1, 87.4, and 91.7%, respectively.

From a whole year view, the estimated total premature mortalities from all non-accidental causes due to surface O_3 exposure over the SCB in 2019 and 2020 are 16,772 and 18,301, respectively (Tables S4 and S5). All O_3 induced diseases within May-June 2019 account for about ~ 17.0% of those in the whole year 2019, and this percentage reaches up to ~ 30.0% in 2020 (Figure S10). The total premature mortalities from all non-accidental causes due to surface O_3 exposure over the SCB has increased by 1528 in the whole year 2020 vs. 2019 (Figure S11), which is 40.8% lower than that within May-June 2020 vs. 2019 (i.e., 2581). This indicates that the O_3 level over the SCB showed an overall decreasing change rate in all months except May-June in 2020 vs. 2019, which resulted in a decrease (by 1053) in O_3 induced diseases in the period.

We further investigated the O_3 induced diseases in the two most densely populated cities over the SCB (i.e., Chengdu and Chongqing) during May-June in 2019 and 2020. The premature mortalities from all O_3 induced diseases in 2020 vs. 2019 in each city are dependent on regional population, surface O_3 level, and enhancement level (equation (9)). With the largest populations and highest O_3 enhancements, the estimated total premature mortalities in Chengdu and Chongqing accounted for 46.9% of total O_3 induced mortalities over the SCB during May-June 2020 (Figure 8 (b)-(c)). Since the O_3 levels and enhancement in Chengdu are larger than those in Chongqing, the total O_3 induced mortalities in Chengdu are larger even with smaller population. The change rates for all O_3 induced diseases are about 75% in Chengdu and 160% in Chongqing during May-June 2020 vs. 2019, which are much higher than the enhancement of ozone levels in the two cities (29.9 %). In order to reduce the O_3 induced health risk, strident O_3 control policies are necessary in

densely populated cities.

7 Conclusions

Understanding the drivers and health risks of surface high O_3 events has a strong implication for O_3 mitigation purpose. After a continuous increase in surface O_3 level from 2013 to 2019, the overall summertime O_3 concentration across China showed a significant reduction in 2020. In contrast to this overall reduction in surface O_3 level across China, unexpected surface O_3 enhancements of 10.2 ± 0.8 ppbv (23%) were observed in May-June 2020 vs. 2019 over the Sichuan basin (SCB), China. In this study, we have used high resolution nested-grid GEOS-Chem simulation, the eXtreme Gradient Boosting (XGBoost) machine learning method and the exposure−response relationship to determine the drivers and evaluated the health risks of the unexpected surface O_3 enhancements.

By iteratively training and correcting the GEOS-Chem model-to-measurement discrepancies, the GEOS-Chem-XGBoost model significantly improves the prediction of surface O_3 concentrations compared to the GEOS-Chem. It shows a bias of 0.5 ± 0.3 ppbv against all O_3 measurements over the SCB. As a result, the overall GEOS-Chem-XGBoost model performance is acceptable and can support further investigation of the drivers of the unexpected surface O_3 enhancements over the SCB in May-June 2020. The results show that changes in anthropogenic emissions caused 0.9 ± 0.1 ppbv of O_3 reduction and changes in meteorology caused 11.1 ± 0.7 ppbv of O_3 increase. The meteorology-induced surface O_3 increase is mainly attributed to an increase in temperature and the decreases in precipitation, specific humidity and cloud fractions over the SCB and surrounding regions in 2020 vs. 2019 levels. These changes in meteorology combined with the complex SCB basin effect enhanced biogenic emissions of VOCs and NO_x, speeded up O_3 chemical production, and inhabited the ventilation of O_3 and its precursors, and therefore caused the surface O_3 enhancements over the SCB.

The unexpected surface O_3 enhancements over the SCB in May-June 2020 vs. 2019 result in dramatically higher health risks. The estimated total premature mortalities due to the unexpected surface O_3 enhancements over the SCB during May-June 2020 is 5455, which is 89.8% higher than that in the same period in 2019 (i.e., 2874). We further investigated the O_3 induced diseases in the two most densely populated cities over the SCB (i.e., Chengdu and Chongqing) during May-June in 2019 and 2020. With largest populations and highest O_3 enhancements, the estimated total premature mortalities in Chengdu and Chongqing accounted for 46.9% of total O_3 induced mortalities over the SCB. The change rates for all O_3 induced diseases are about 75% in Chengdu and 160% in Chongqing during May-June 2020 vs. 2019, which are much higher than the enhancement of ozone levels in the two cities (29.9 %). In order to reduce the O_3 induced health risks, strident O_3 control policies are necessary in densely populated cities.

Code and data availability. Surface O_3 measurements over the SCB are from http://www.cnemc.cn/en/. All other data are available on request of YS (ywsun@aiofm.ac.cn)

Author contributions. YS designed the study and wrote the paper. HY carried out the GEOS-Chem simulations and GEOS-Chem-XGBoost training and evaluation. BZ constructed the latest MEIC emission inventory. XL, JN, MP, CL, and YT provided constructive comments.

Competing interests. None.

Acknowledgements. This work is jointly supported by the National Key Research and Development Program of China (No.2019YFC0214802), the Youth Innovation Promotion Association, CAS (No.2019434), and the Sino-German Mobility programme (M-0036). The authors would also like to thank Prof. Wernli Heini and the two anonymous referees for their valuable comments that improved the quality of this paper.

References

Akimoto, H., Mori, Y., Sasaki, K., Nakanishi, H., Ohizumi, T., and Itano, Y.: Analysis of monitoring data of ground-level ozone in Japan for long-term trend during 1990–2010: Causes of temporal and spatial variation, Atmos Environ, 102, 302-310, https://doi.org/10.1016/j.atmosenv.2014.12.001, 2015.

Anenberg, S. C., Horowitz, L. W., Tong, D. Q., and West, J. J.: An Estimate of the Global Burden of Anthropogenic Ozone and Fine Particulate Matter on Premature Human Mortality Using Atmospheric Modeling, Environmental Health Perspectives, 118, 1189-1195, 2010.

Atkinson, R.: Atmospheric chemistry of VOCs and NOx, Atmos Environ, 34, 2063-2101, 2000.

Bey, I., Jacob, D. J., Yantosca, R. M., Logan, J. A., Field, B. D., Fiore, A. M., Li, Q. B., Liu, H. G. Y., Mickley, L. J., and Schultz, M. G.: Global modeling of tropospheric chemistry with assimilated meteorology: Model description and evaluation, J Geophys Res-Atmos, 106, 23073-23095, Doi 10.1029/2001jd000807, 2001.

Bian, H. S., and Prather, M. J.: Fast-J2: Accurate simulation of stratospheric photolysis in global chemical models, J Atmos Chem, 41, 281-296, 2002.

Brauer, M., Freedman, G., Frostad, J., van Donkelaar, A., Martin, R. V., Dentener, F., van Dingenen, R., Estep, K., Amini, H., Apte, J. S., Balakrishnan, K., Barregard, L., Broday, D., Feigin, V., Ghosh, S., Hopke, P. K., Knibbs, L. D., Kokubo, Y., Liu, Y., Ma, S. F., Morawska, L., Sangrador, J. L. T., Shaddick, G., Anderson, H. R., Vos, T., Forouzanfar, M. H., Burnett, R. T., and Cohen, A.: Ambient Air Pollution Exposure Estimation for the Global Burden of Disease 2013, Environmental Science & Technology, 50, 79-88, 2016.

Chen, D., Wang, Y., McElroy, M. B., He, K., Yantosca, R. M., and Le Sager, P.: Regional CO pollution and export in China simulated by the high-resolution nested-grid GEOS-Chem model, Atmos Chem Phys, 9, 3825-3839, 2009.

Chen, X. R., Wang, H. C., Lu, K. D., Li, C. M., Zhai, T. Y., Tan, Z. F., Ma, X. F., Yang, X. P., Liu, Y. H., Chen, S. Y., Dong, H. B., Li, X., Wu, Z. J., Hu, M., Zeng, L. M., and Zhang, Y. H.: Field Determination of Nitrate Formation Pathway in Winter Beijing, Environmental Science & Technology, 54, 9243-9253, 2020.

Cohen, A. J., Anderson, H. R., Ostro, B., Pandey, K. D., Krzyzanowski, M., Künzli, N., Gutschmidt, K., Pope, A., Romieu, I., Samet, J. M., and Smith, K.: Urban air pollution, in: Comparative quantification of health risks, Global and regional burden of disease attributable to selected major risk factors, World Health Organization, Geneva, 1, 2004.

Cooper, O. R.: Detecting the fingerprints of observed climate change on surface ozone variability, Sci Bull, 64, 359-360, 2019.

Eastham, S. D., Weisenstein, D. K., and Barrett, S. R. H.: Development and evaluation of the unified tropospheric-stratospheric chemistry extension (UCX) for the global chemistry-transport

model GEOS-Chem, Atmos Environ, 89, 52-63, 2014.
Fleming, Z. L., Doherty, R. M., von Schneidemesser, E., Malley, C. S., Cooper, O. R., Pinto, J. P., Colette, A., Xu, X. B., Simpson, D., Schultz, M. G., Lefohn, A. S., Hamad, S., Moolla, R., Solberg, S., and Feng, Z. Z.: Tropospheric Ozone Assessment Report: Present-day ozone distribution and trends relevant to human health, Elementa-Sci Anthrop, 6, 2018.
Fu, T.-M., Zheng, Y., Paulot, F., Mao, J., and Yantosca, R. M.: Positive but variable sensitivity of August surface ozone to large-scale warming in the southeast United States, Nat Clim Change, 5, 454-458, 10.1038/nclimate2567, 2015.
Giglio, L., Randerson, J. T., and van der Werf, G. R.: Analysis of daily, monthly, and annual burned area using the fourth-generation global fire emissions database (GFED4), J Geophys Res-Biogeo, 118, 317-328, 10.1002/jgrg.20042, 2013.
Guenther, A., Karl, T., Harley, P., Wiedinmyer, C., Palmer, P. I., and Geron, C.: Estimates of global terrestrial isoprene emissions using MEGAN (Model of Emissions of Gases and Aerosols from Nature), Atmos Chem Phys, 6, 3181-3210, 2006.
Guenther, A. B., Jiang, X., Heald, C. L., Sakulyanontvittaya, T., Duhl, T., Emmons, L. K., and Wang, X.: The Model of Emissions of Gases and Aerosols from Nature version 2.1 (MEGAN2.1): an extended and updated framework for modeling biogenic emissions, Geosci Model Dev, 5, 1471-1492, 2012.
He, J. J., Gong, S. L., Yu, Y., Yu, L. J., Wu, L., Mao, H. J., Song, C. B., Zhao, S. P., Liu, H. L., Li, X. Y., and Li, R. P.: Air pollution characteristics and their relation to meteorological conditions during 2014-2015 in major Chinese cities, Environmental Pollution, 223, 484-496, 2017.
Hoesly, R. M., Smith, S. J., Feng, L. Y., Klimont, Z., Janssens-Maenhout, G., Pitkanen, T., Seibert, J. J., Vu, L., Andres, R. J., Bolt, R. M., Bond, T. C., Dawidowski, L., Kholod, N., Kurokawa, J., Li, M., Liu, L., Lu, Z. F., Moura, M. C. P., O'Rourke, P. R., and Zhang, Q.: Historical (1750-2014) anthropogenic emissions of reactive gases and aerosols from the Community Emissions Data System (CEDS), Geosci Model Dev, 11, 369-408, 10.5194/gmd-11-369-2018, 2018.
Hudman, R. C., Russell, A. R., Valin, L. C., and Cohen, R. C.: Interannual variability in soil nitric oxide emissions over the United States as viewed from space, Atmos. Chem. Phys., 10, 9943-9952, 10.5194/acp-10-9943-2010, 2010.
Im, U., Markakis, K., Poupkou, A., Melas, D., Unal, A., Gerasopoulos, E., Daskalakis, N., Kindap, T., and Kanakidou, M.: The impact of temperature changes on summer time ozone and its precursors in the Eastern Mediterranean, Atmos Chem Phys, 11, 3847-3864, 2011.
Jin, X., Fiore, A. M., Murray, L. T., Valin, L. C., Lamsal, L. N., Duncan, B., Folkert Boersma, K., De Smedt, I., Abad, G. G., Chance, K., and Tonnesen, G. S.: Evaluating a Space-Based Indicator of Surface Ozone-NO_x-VOC Sensitivity Over Midlatitude Source Regions and Application to Decadal Trends, Journal of Geophysical Research: Atmospheres, 122, 10,439-410,461, https://doi.org/10.1002/2017JD026720, 2017.
Jin, X. M., and Holloway, T.: Spatial and temporal variability of ozone sensitivity over China observed from the Ozone Monitoring Instrument, J Geophys Res-Atmos, 120, 7229-7246, 2015.
Kalabokas, P. D., Thouret, V., Cammas, J. P., Volz-Thomas, A., Boulanger, D., and Repapis, C. C.: The geographical distribution of meteorological parameters associated with high and low summer ozone levels in the lower troposphere and the boundary layer over the eastern Mediterranean (Cairo case), Tellus B, 67, 2015.

Keller, C. A., Evans, M. J., Knowland, K. E., Hasenkopf, C. A., Modekurty, S., Lucchesi, R. A., Oda, T., Franca, B. B., Mandarino, F. C., Díaz Suárez, M. V., Ryan, R. G., Fakes, L. H., and Pawson, S.: Global impact of COVID-19 restrictions on the surface concentrations of nitrogen dioxide and ozone, Atmos. Chem. Phys., 21, 3555-3592, 10.5194/acp-21-3555-2021, 2021.

Lee, Y. C., Shindell, D. T., Faluvegi, G., Wenig, M., Lam, Y. F., Ning, Z., Hao, S., and Lai, C. S.: Increase of ozone concentrations, its temperature sensitivity and the precursor factor in South China, Tellus B, 66, 2014.

Lefohn, A. S., Wernli, H., Shadwick, D., Oltmans, S. J., and Shapiro, M.: Quantifying the importance of stratospheric-tropospheric transport on surface ozone concentrations at high- and low-elevation monitoring sites in the United States, Atmos Environ, 62, 646-656, 2012.

Lelieveld, J., and Crutzen, P. J.: Influences of Cloud Photochemical Processes on Tropospheric Ozone, Nature, 343, 227-233, 1990.

Lelieveld, J., Barlas, C., Giannadaki, D., and Pozzer, A.: Model calculated global, regional and megacity premature mortality due to air pollution, Atmos Chem Phys, 13, 7023-7037, 2013.

Li, J., Wang, Z., Wang, X., Yamaji, K., Takigawa, M., Kanaya, Y., Pochanart, P., Liu, Y., Irie, H., Hu, B., Tanimoto, H., and Akimoto, H.: Impacts of aerosols on summertime tropospheric photolysis frequencies and photochemistry over Central Eastern China, Atmos Environ, 45, 1817-1829, 2011.

Li, J., Chen, X. S., Wang, Z. F., Du, H. Y., Yang, W. Y., Sun, Y. L., Hu, B., Li, J. J., Wang, W., Wang, T., Fu, P. Q., and Huang, H. L.: Radiative and heterogeneous chemical effects of aerosols on ozone and inorganic aerosols over East Asia, Sci Total Environ, 622, 1327-1342, 2018.

Li, K., Jacob, D. J., Liao, H., Shen, L., Zhang, Q., and Bates, K. H.: Anthropogenic drivers of 2013–2017 trends in summer surface ozone in China, Proceedings of the National Academy of Sciences, 116, 422-427, 10.1073/pnas.1812168116, 2019a.

Li, K., Jacob, D. J., Liao, H., Zhu, J., Shah, V., Shen, L., Bates, K. H., Zhang, Q., and Zhai, S.: A two-pollutant strategy for improving ozone and particulate air quality in China, Nat Geosci, 12, 906-910, 10.1038/s41561-019-0464-x, 2019b.

Li, M., Zhang, Q., Kurokawa, J., Woo, J. H., He, K. B., Lu, Z. F., Ohara, T., Song, Y., Streets, D. G., Carmichael, G. R., Cheng, Y. F., Hong, C. P., Huo, H., Jiang, X. J., Kang, S. C., Liu, F., Su, H., and Zheng, B.: MIX: a mosaic Asian anthropogenic emission inventory under the international collaboration framework of the MICS-Asia and HTAP, Atmos Chem Phys, 17, 935-963, 10.5194/acp-17-935-2017, 2017.

Li, T. T., Yan, M. L., Ma, W. J., Ban, J., Liu, T., Lin, H. L., and Liu, Z. R.: Short-term effects of multiple ozone metrics on daily mortality in a megacity of China, Environ Sci Pollut R, 22, 8738-8746, 2015.

Lim, S. S., Vos, T., Flaxman, A. D., Danaei, G., Shibuya, K., Adair-Rohani, H., Amann, M., Anderson, H. R., Andrews, K. G., Aryee, M., Atkinson, C., Bacchus, L. J., Bahalim, A. N., Balakrishnan, K., Balmes, J., Barker-Collo, S., Baxter, A., Bell, M. L., Blore, J. D., Blyth, F., Bonner, C., Borges, G., Bourne, R., Boussinesq, M., Brauer, M., Brooks, P., Bruce, N. G., Brunekreef, B., Bryan-Hancock, C., Bucello, C., Buchbinder, R., Bull, F., Burnett, R. T., Byers, T. E., Calabria, B., Carapetis, J., Carnahan, E., Chafe, Z., Charlson, F., Chen, H. L., Chen, J. S., Cheng, A. T. A., Child, J. C., Cohen, A., Colson, K. E., Cowie, B. C., Darby, S., Darling, S., Davis, A., Degenhardt, L., Dentener, F., Des Jarlais, D. C., Devries, K., Dherani, M., Ding, E. L., Dorsey, E. R., Driscoll, T., Edmond, K., Ali, S. E., Engell, R. E., Erwin, P. J., Fahimi, S.,

Falder, G., Farzadfar, F., Ferrari, A., Finucane, M. M., Flaxman, S., Fowkes, F. G. R., Freedman, G., Freeman, M. K., Gakidou, E., Ghosh, S., Giovannucci, E., Gmel, G., Graham, K., Grainger, R., Grant, B., Gunnell, D., Gutierrez, H. R., Hall, W., Hoek, H. W., Hogan, A., Hosgood, H. D., Hoy, D., Hu, H., Hubbell, B. J., Hutchings, S. J., Ibeanusi, S. E., Jacklyn, G. L., Jasrasaria, R., Jonas, J. B., Kan, H. D., Kanis, J. A., Kassebaum, N., Kawakami, N., Khang, Y. H., Khatibzadeh, S., Khoo, J. P., Kok, C., Laden, F., Lalloo, R., Lan, Q., Lathlean, T., Leasher, J. L., Leigh, J., Li, Y., Lin, J. K., Lipshultz, S. E., London, S., Lozano, R., Lu, Y., Mak, J., Malekzadeh, R., Mallinger, L., Marcenes, W., March, L., Marks, R., Martin, R., McGale, P., McGrath, J., Mehta, S., Mensah, G. A., Merriman, T. R., Micha, R., Michaud, C., Mishra, V., Hanafiah, K. M., Mokdad, A. A., Morawska, L., Mozaffarian, D., Murphy, T., Naghavi, M., Neal, B., Nelson, P. K., Nolla, J. M., Norman, R., Olives, C., Omer, S. B., Orchard, J., Osborne, R., Ostro, B., Page, A., Pandey, K. D., Parry, C. D. H., Passmore, E., Patra, J., Pearce, N., Pelizzari, P. M., Petzold, M., Phillips, M. R., Pope, D., Pope, C. A., Powles, J., Rao, M., Razavi, H., Rehfuess, E. A., Rehm, J. T., Ritz, B., Rivara, F. P., Roberts, T., Robinson, C., Rodriguez-Portales, J. A., Romieu, I., Room, R., Rosenfeld, L. C., Roy, A., Rushton, L., Salomon, J. A., Sampson, U., Sanchez-Riera, L., Sanman, E., Sapkota, A., Seedat, S., Shi, P. L., Shield, K., Shivakoti, R., Singh, G. M., Sleet, D. A., Smith, E., Smith, K. R., Stapelberg, N. J. C., Steenland, K., Stockl, H., Stovner, L. J., Straif, K., Straney, L., Thurston, G. D., Tran, J. H., Van Dingenen, R., van Donkelaar, A., Veerman, J. L., Vijayakumar, L., Weintraub, R., Weissman, M. M., White, R. A., Whiteford, H., Wiersma, S. T., Wilkinson, J. D., Williams, H. C., Williams, W., Wilson, N., Woolf, A. D., Yip, P., Zielinski, J. M., Lopez, A. D., Murray, C. J. L., and Ezzati, M.: A comparative risk assessment of burden of disease and injury attributable to 67 risk factors and risk factor clusters in 21 regions, 1990-2010: a systematic analysis for the Global Burden of Disease Study 2010, Lancet, 380, 2224-2260, 2012.

Lin, J. T., Patten, K. O., Hayhoe, K., Liang, X. Z., and Wuebbles, D. J.: Effects of future climate and biogenic emissions changes on surface ozone over the United States and China, Journal of Applied Meteorology and Climatology, 47, 1888-1909, 2008.

Lin, J. T., and McElroy, M. B.: Impacts of boundary layer mixing on pollutant vertical profiles in the lower troposphere: Implications to satellite remote sensing, Atmos Environ, 44, 1726-1739, 2010.

Liu, H., Liu, S., Xue, B. R., Lv, Z. F., Meng, Z. H., Yang, X. F., Xue, T., Yu, Q., and He, K. B.: Ground-level ozone pollution and its health impacts in China, Atmos Environ, 173, 223-230, 2018.

Liu, H. Y., Jacob, D. J., Bey, I., and Yantosca, R. M.: Constraints from Pb-210 and Be-7 on wet deposition and transport in a global three-dimensional chemical tracer model driven by assimilated meteorological fields, J Geophys Res-Atmos, 106, 12109-12128, Doi 10.1029/2000jd900839, 2001.

Liu, H. Y., Jacob, D. J., Bey, I., Yantosca, R. M., Duncan, B. N., and Sachse, G. W.: Transport pathways for Asian pollution outflow over the Pacific: Interannual and seasonal variations, J Geophys Res-Atmos, 108, 2003.

Liu, Y. M., and Wang, T.: Worsening urban ozone pollution in China from 2013 to 2017-Part 1: The complex and varying roles of meteorology, Atmos Chem Phys, 20, 6305-6321, 2020a.

Liu, Y. M., and Wang, T.: Worsening urban ozone pollution in China from 2013 to 2017-Part 2: The effects of emission changes and implications for multi-pollutant control, Atmos Chem Phys,

20, 6323-6337, 2020b.
Lou, S., Liao, H., and Zhu, B.: Impacts of aerosols on surface-layer ozone concentrations in China through heterogeneous reactions and changes in photolysis rates, Atmos Environ, 85, 123-138, https://doi.org/10.1016/j.atmosenv.2013.12.004, 2014.
Lu, K. D., Rohrer, F., Holland, F., Fuchs, H., Bohn, B., Brauers, T., Chang, C. C., Haseler, R., Hu, M., Kita, K., Kondo, Y., Li, X., Lou, S. R., Nehr, S., Shao, M., Zeng, L. M., Wahner, A., Zhang, Y. H., and Hofzumahaus, A.: Observation and modelling of OH and HO_2 concentrations in the Pearl River Delta 2006: a missing OH source in a VOC rich atmosphere, Atmos Chem Phys, 12, 1541-1569, 2012.
Lu, K. D., Fuchs, H., Hofzumahaus, A., Tan, Z. F., Wang, H. C., Zhang, L., Schmitt, S. H., Rohrer, F., Bohn, B., Broch, S., Dong, H. B., Gkatzelis, G. I., Hohaus, T., Holland, F., Li, X., Liu, Y., Liu, Y. H., Ma, X. F., Novelli, A., Schlag, P., Shao, M., Wu, Y. S., Wu, Z. J., Zeng, L. M., Hu, M., Kiendler-Scharr, A., Wahner, A., and Zhang, Y. H.: Fast Photochemistry in Wintertime Haze: Consequences for Pollution Mitigation Strategies, Environmental Science & Technology, 53, 10676-10684, 2019a.
Lu, K. D., Guo, S., Tan, Z. F., Wang, H. C., Shang, D. J., Liu, Y. H., Li, X., Wu, Z. J., Hu, M., and Zhang, Y. H.: Exploring atmospheric free-radical chemistry in China: the self-cleansing capacity and the formation of secondary air pollution, Natl Sci Rev, 6, 579-594, 2019b.
Lu, X., Hong, J., Zhang, L., Cooper, O. R., Schultz, M. G., Xu, X., Wang, T., Gao, M., Zhao, Y., and Zhang, Y.: Severe Surface Ozone Pollution in China: A Global Perspective, Environ Sci Tech Let, 5, 487-494, 10.1021/acs.estlett.8b00366, 2018.
Lu, X., Zhang, L., Chen, Y., Zhou, M., Zheng, B., Li, K., Liu, Y., Lin, J., Fu, T. M., and Zhang, Q.: Exploring 2016–2017 surface ozone pollution over China: source contributions and meteorological influences, Atmos. Chem. Phys., 19, 8339-8361, 10.5194/acp-19-8339-2019, 2019c.
Lu, X., Zhang, L., and Shen, L.: Meteorology and Climate Influences on Tropospheric Ozone: a Review of Natural Sources, Chemistry, and Transport Patterns, Current Pollution Reports, 5, 238-260, 10.1007/s40726-019-00118-3, 2019d.
Lu, X., Zhang, L., Wang, X., Gao, M., Li, K., Zhang, Y., Yue, X., and Zhang, Y.: Rapid Increases in Warm-Season Surface Ozone and Resulting Health Impact in China Since 2013, Environ Sci Tech Let, 7, 240-247, 10.1021/acs.estlett.0c00171, 2020.
Lu, X., Ye, X., Zhou, M., Zhao, Y., Weng, H., Kong, H., Li, K., Gao, M., Zheng, B., Lin, J., Zhou, F., Zhang, Q., Wu, D., Zhang, L., and Zhang, Y.: The underappreciated role of agricultural soil nitrogen oxide emissions in ozone pollution regulation in North China, Nature Communications, 12, 5021, 10.1038/s41467-021-25147-9, 2021.
Lundberg, S. M., and Lee, S.-I.: A Unified Approach to Interpreting Model Predictions, https://arxiv.org/pdf/1705.07874.pdf, 2017.
Lundberg, S. M., Erion, G., Chen, H., DeGrave, A., Prutkin, J. M., Nair, B., Katz, R., Himmelfarb, J., Bansal, N., and Lee, S.-I.: From local explanations to global understanding with explainable AI for trees, Nature Machine Intelligence, 2, 56-67, 10.1038/s42256-019-0138-9, 2020.
McDuffie, E. E., Smith, S. J., O'Rourke, P., Tibrewal, K., Venkataraman, C., Marais, E. A., Zheng, B., Crippa, M., Brauer, M., and Martin, R. V.: A global anthropogenic emission inventory of atmospheric pollutants from sector- and fuel-specific sources (1970–2017): an application of the Community Emissions Data System (CEDS), Earth Syst. Sci. Data, 12, 3413-3442,

10.5194/essd-12-3413-2020, 2020.
Murray, L. T., Jacob, D. J., Logan, J. A., Hudman, R. C., and Koshak, W. J.: Optimized regional and interannual variability of lightning in a global chemical transport model constrained by LIS/OTD satellite data, Journal of Geophysical Research: Atmospheres, 117, https://doi.org/10.1029/2012JD017934, 2012.
Philip, S., Martin, R. V., and Keller, C. A.: Sensitivity of chemistry-transport model simulations to the duration of chemical and transport operators: a case study with GEOS-Chem v10-01, Geosci Model Dev, 9, 1683-1695, 2016.
Sanchez-Ccoyllo, O. R., Ynoue, R. Y., Martins, L. D., and Andrade, M. D.: Impacts of ozone precursor limitation and meteorological variables on ozone concentration in Sao Paulo, Brazil, Atmos Environ, 40, S552-S562, 2006.
Seinfeld, J. H., and Pandis, S. N.: Atmospheric chemistry and physics: from air pollution to climate change, John Wiley & Sons, 2016.
Shan, W. P., Yin, Y. Q., Zhang, J. D., and Ding, Y. P.: Observational study of surface ozone at an urban site in East China, Atmos Res, 89, 252-261, 2008.
Skerlak, B., Sprenger, M., and Wernli, H.: A global climatology of stratosphere-troposphere exchange using the ERA-Interim data set from 1979 to 2011, Atmos Chem Phys, 14, 913-937, 2014.
Stadtler, S., Simpson, D., Schroder, S., Taraborrelli, D., Bott, A., and Schultz, M.: Ozone impacts of gas-aerosol uptake in global chemistry transport models, Atmos Chem Phys, 18, 3147-3171, 2018.
Steinbrecht, W., Kubistin, D., Plass-Dulmer, C., Davies, J., Tarasick, D. W., von der Gathen, P., Deckelmann, H., Jepsen, N., Kivi, R., Lyall, N., Palm, M., Notholt, J., Kois, B., Oelsner, P., Allaart, M., Piters, A., Gill, M., Van Malderen, R., Delcloo, A. W., Sussmann, R., Mahieu, E., Servais, C., Romanens, G., Stubi, R., Ancellet, G., Godin-Beekmann, S., Yamanouchi, S., Strong, K., Johnson, B., Cullis, P., Petropavlovskikh, I., Hannigan, J. W., Hernandez, J. L., Rodriguez, A. D., Nakano, T., Chouza, F., Leblanc, T., Torres, C., Garcia, O., Rohling, A. N., Schneider, M., Blumenstock, T., Tully, M., Paton-Walsh, C., Jones, N., Querel, R., Strahan, S., Stauffer, R. M., Thompson, A. M., Inness, A., Engelen, R., Chang, K. L., and Cooper, O. R.: COVID-19 Crisis Reduces Free Tropospheric Ozone Across the Northern Hemisphere, Geophys Res Lett, 48, 2021.
Steinfeld, J. I.: Atmospheric Chemistry and Physics: From Air Pollution to Climate Change, Environment: Science and Policy for Sustainable Development, 40, 26-26, 10.1080/00139157.1999.10544295, 1998.
Stohl, A., Wernli, H., James, P., Bourqui, M., Forster, C., Liniger, M. A., Seibert, P., and Sprenger, M.: A new perspective of stratosphere-troposphere exchange, B Am Meteorol Soc, 84, 1565-+, 2003.
Streets, D. G., Canty, T., Carmichael, G. R., de Foy, B., Dickerson, R. R., Duncan, B. N., Edwards, D. P., Haynes, J. A., Henze, D. K., Houyoux, M. R., Jacobi, D. J., Krotkov, N. A., Lamsal, L. N., Liu, Y., Lu, Z. F., Martini, R. V., Pfister, G. G., Pinder, R. W., Salawitch, R. J., and Wechti, K. J.: Emissions estimation from satellite retrievals: A review of current capability, Atmos Environ, 77, 1011-1042, 2013.
Sun, Y., Wang, Y., and Zhang, C.: Vertical observations and analysis of $PM_{2.5}$, O_3, and NO_x at Beijing and Tianjin from towers during summer and Autumn 2006, Advances in Atmospheric Sciences,

27, 123, 10.1007/s00376-009-8154-z, 2009.
Sun, Y., Yin, H., Liu, C., Mahieu, E., Notholt, J., Té, Y., Lu, X., Palm, M., Wang, W., Shan, C., Hu, Q., Qin, M., Tian, Y., and Zheng, B.: The reduction in C2H6 from 2015 to 2020 over Hefei, eastern China, points to air quality improvement in China, Atmos. Chem. Phys., 21, 11759-11779, 10.5194/acp-21-11759-2021, 2021a.
Sun, Y., Yin, H., Liu, C., Zhang, L., Cheng, Y., Palm, M., Notholt, J., Lu, X., Vigouroux, C., Zheng, B., Wang, W., Jones, N., Shan, C., Qin, M., Tian, Y., Hu, Q., Meng, F., and Liu, J.: Mapping the drivers of formaldehyde (HCHO) variability from 2015 to 2019 over eastern China: insights from Fourier transform infrared observation and GEOS-Chem model simulation, Atmos. Chem. Phys., 21, 6365-6387, 10.5194/acp-21-6365-2021, 2021b.
Sun, Y., Yin, H., Cheng, Y., Zhang, Q., Zheng, B., Notholt, J., Lu, X., Liu, C., Tian, Y., and Liu, J.: Quantifying variability, source, and transport of CO in the urban areas over the Himalayas and Tibetan Plateau, Atmos. Chem. Phys., 21, 9201-9222, 10.5194/acp-21-9201-2021, 2021c.
Sun, Y. W., Liu, C., Palm, M., Vigouroux, C., Notholt, J., Hui, Q. H., Jones, N., Wang, W., Su, W. J., Zhang, W. Q., Shan, C. G., Tian, Y., Xu, X. W., De Maziere, M., Zhou, M. Q., and Liu, J. G.: Ozone seasonal evolution and photochemical production regime in the polluted troposphere in eastern China derived from high-resolution Fourier transform spectrometry (FTS) observations, Atmos Chem Phys, 18, 14569-14583, 2018.
Tarvainen, V., Hakola, H., Hellen, H., Back, J., Hari, P., and Kulmala, M.: Temperature and light dependence of the VOC emissions of Scots pine, Atmos Chem Phys, 5, 989-998, 2005.
Van Dingenen, R., Dentener, F. J., Raes, F., Krol, M. C., Emberson, L., and Cofala, J.: The global impact of ozone on agricultural crop yields under current and future air quality legislation, Atmos Environ, 43, 604-618, 2009.
Wang, H. C., and Lu, K. D.: Monitoring Ambient Nitrate Radical by Open-Path Cavity-Enhanced Absorption Spectroscopy, Anal Chem, 91, 10687-10693, 2019.
Wang, H. C., Chen, X. R., Lu, K. D., Tan, Z. F., Ma, X. F., Wu, Z. J., Li, X., Liu, Y. H., Shang, D. J., Wu, Y. S., Zeng, L. M., Hu, M., Schmitt, S., Kiendler-Scharr, A., Wahner, A., and Zhang, Y. H.: Wintertime N2O5 uptake coefficients over the North China Plain, Sci Bull, 65, 765-774, 2020a.
Wang, H. Y., Wang, W., Huang, X., and Ding, A. J.: Impacts of stratosphere-to-troposphere-transport on summertime surface ozone over eastern China, Sci Bull, 65, 276-279, 2020b.
Wang, P., Wang, T., and Ying, Q.: Regional source apportionment of summertime ozone and its precursors in the megacities of Beijing and Shanghai using a source-oriented chemical transport model, Atmos Environ, 224, 2020c.
Wang, P., Shen, J. Y., Xia, M., Sun, S. D., Zhang, Y. L., Zhang, H. L., and Wang, X. M.: Unexpected enhancement of ozone exposure and health risks during National Day in China, Atmos Chem Phys, 21, 10347-10356, 2021.
Wang, T., Xue, L. K., Brimblecombe, P., Lam, Y. F., Li, L., and Zhang, L.: Ozone pollution in China: A review of concentrations, meteorological influences, chemical precursors, and effects, Sci Total Environ, 575, 1582-1596, 2017.
Wang, X. Y., Wu, Y. T., Randel, W., and Tilmes, S.: Stratospheric contribution to the summertime high surface ozone events over the western united states, Environ Res Lett, 15, 2020d.
Wesely, M. L.: Parameterization of Surface Resistances to Gaseous Dry Deposition in Regional-Scale Numerical-Models, Atmos Environ, 23, 1293-1304, Doi 10.1016/0004-6981(89)90153-

4, 1989.
Wirth, V., and Egger, J.: Diagnosing extratropical synoptic-scale stratosphere-troposphere exchange: A case study, Q J Roy Meteor Soc, 125, 635-655, 1999.
Xing, J., Wang, J. D., Mathur, R., Wang, S. X., Sarwar, G., Pleim, J., Hogrefe, C., Zhang, Y. Q., Jiang, J. K., Wong, D. C., and Hao, J. M.: Impacts of aerosol direct effects on tropospheric ozone through changes in atmospheric dynamics and photolysis rates, Atmos Chem Phys, 17, 9869-9883, 2017.
Yin, H., Sun, Y., Liu, C., Zhang, L., Lu, X., Wang, W., Shan, C., Hu, Q., Tian, Y., Zhang, C., Su, W., Zhang, H., Palm, M., Notholt, J., and Liu, J.: FTIR time series of stratospheric NO_2 over Hefei, China, and comparisons with OMI and GEOS-Chem model data, Opt Express, 27, A1225-A1240, 10.1364/OE.27.0A1225, 2019.
Yin, H., Sun, Y., Liu, C., Lu, X., Smale, D., Blumenstock, T., Nagahama, T., Wang, W., Tian, Y., Hu, Q., Shan, C., Zhang, H., and Liu, J.: Ground-based FTIR observation of hydrogen chloride (HCl) over Hefei, China, and comparisons with GEOS-Chem model data and other ground-based FTIR stations data, Opt Express, 28, 8041-8055, 10.1364/OE.384377, 2020.
Yin, H., Liu, C., Hu, Q., Liu, T., Wang, S., Gao, M., Xu, S., Zhang, C., and Su, W.: Opposite impact of emission reduction during the COVID-19 lockdown period on the surface concentrations of $PM_{2.5}$ and O_3 in Wuhan, China, Environmental Pollution, 289, 117899, https://doi.org/10.1016/j.envpol.2021.117899, 2021.
Yin, P., Chen, R. J., Wang, L. J., Meng, X., Liu, C., Niu, Y., Lin, Z. J., Liu, Y. N., Liu, J. M., Qi, J. L., You, J. L., Zhou, M. G., and Kan, H. D.: Ambient Ozone Pollution and Daily Mortality: A Nationwide Study in 272 Chinese Cities, Environmental Health Perspectives, 125, 2017.
Yin, H., Lu, X., Sun, Y., Li, K., Gao, M., Zheng, B., and Liu, C.: Unprecedented decline in summertime surface ozone over eastern China in 2020 comparably attributable to anthropogenic emission reductions and meteorology, Environ Res Lett, under review, 2021.
Young, P. J., Naik, V., Fiore, A. M., Gaudel, A., Guo, J., Lin, M. Y., Neu, J. L., Parrish, D. D., Rieder, H. E., Schnell, J. L., Tilmes, S., Wild, O., Zhang, L., Ziemke, J., Brandt, J., Delcloo, A., Doherty, R. M., Geels, C., Hegglin, M. I., Hu, L., Im, U., Kumar, R., Luhar, A., Murray, L., Plummer, D., Rodriguez, J., Saiz-Lopez, A., Schultz, M. G., Woodhouse, M. T., and Zeng, G.: Tropospheric Ozone Assessment Report: Assessment of global-scale model performance for global and regional ozone distributions, variability, and trends, Elementa: Science of the Anthropocene, 6, 10.1525/elementa.265, 2018.
Zhang, L. M., Gong, S. L., Padro, J., and Barrie, L.: A size-segregated particle dry deposition scheme for an atmospheric aerosol module, Atmos Environ, 35, 549-560, Doi 10.1016/S1352-2310(00)00326-5, 2001.
Zheng, B., Tong, D., Li, M., Liu, F., Hong, C. P., Geng, G. N., Li, H. Y., Li, X., Peng, L. Q., Qi, J., Yan, L., Zhang, Y. X., Zhao, H. Y., Zheng, Y. X., He, K. B., and Zhang, Q.: Trends in China's anthropogenic emissions since 2010 as the consequence of clean air actions, Atmos Chem Phys, 18, 14095-14111, 2018.
Zheng, B., Zhang, Q., Geng, G. N., Chen, C. H., Shi, Q. R., Cui, M. S., Lei, Y., and He, K. B.: Changes in China's anthropogenic emissions and air quality during the COVID-19 pandemic in 2020, Earth Syst Sci Data, 13, 2895-2907, 2021.
Zou, Q., Song, H., Tang, M. J., and Lu, K. D.: Measurements of HO_2 uptake coefficient on aqueous $(NH_4)_{(2)}SO_4$ aerosol using aerosol flow tube with LIF system, Chinese Chem Lett, 30, 2236-

2240, 2019.

Tables

Table 1. Measurement sites in the SCB city clusters. All sites are organised alphabetically. Population statistics are based on the seventh nationwide population census in 2020 provided by National Bureau of Statistics of China.

Name	Longitude mean	Latitude mean	Altitude mean (km)	Population	Number of sites	Time period
Abazhou	102.21°E	31.91°N	3.5	822,587	3	2015 - present
Bazhong	106.75°E	31.85°N	0.8	2,712,894	4	2015 - present
Chengdu	104.04°E	30.69°N	0.5	20,938,000	10	2015 - present
Chongqing	106.51°E	29.58°N	0.4	32,054,200	21	2015 - present
Dazhou	107.5°E	31.22°N	1.0	5,385,422	5	2015 - present
Deyang	104.39°E	31.12°N	0.5	3,456,161	4	2015 - present
Ganzizhou	101.96°E	30.05°N	3.5	1,107,431	2	2015 - present
Guangan	106.63°E	30.48°N	1.7	3,254,883	6	2015 - present
Guangyuan	105.85°E	32.44°N	2.1	2,305,657	4	2015 - present
Leshan	103.76°E	29.57°N	0.5	3,160,168	4	2015 - present
Liangshanzhou	102.28°E	27.87°N	2.3	4,858,359	5	2015 - present
Luzhou	105.43°E	28.9°N	0.3	4,254,149	4	2015 - present
Meishan	103.85°E	30.07°N	0.8	2,955,219	6	2015 - present
Mianyang	104.73°E	31.48°N	0.7	4,868,243	4	2015 - present
Nanchong	106.09°E	30.8°N	0.3	5,607,565	6	2015 - present
Neijiang	105.05°E	29.59°N	0.5	3,140,678	4	2015 - present
Panzhihua	101.69°E	26.56°N	2.6	1,212,203	5	2015 - present
Suining	105.71°E	30.58°N	0.5	2,814,196	4	2015 - present
Yaan	103.01°E	29.99°N	3.1	1,434,603	4	2015 - present
Yibin	104.62°E	28.78°N	2.0	4,588,804	6	2015 - present
Zigong	104.75°E	29.35°N	0.3	2,489,256	6	2015 - present
Ziyang	104.64°E	30.13°N	0.5	2,308,631	5	2015 - present

Figures

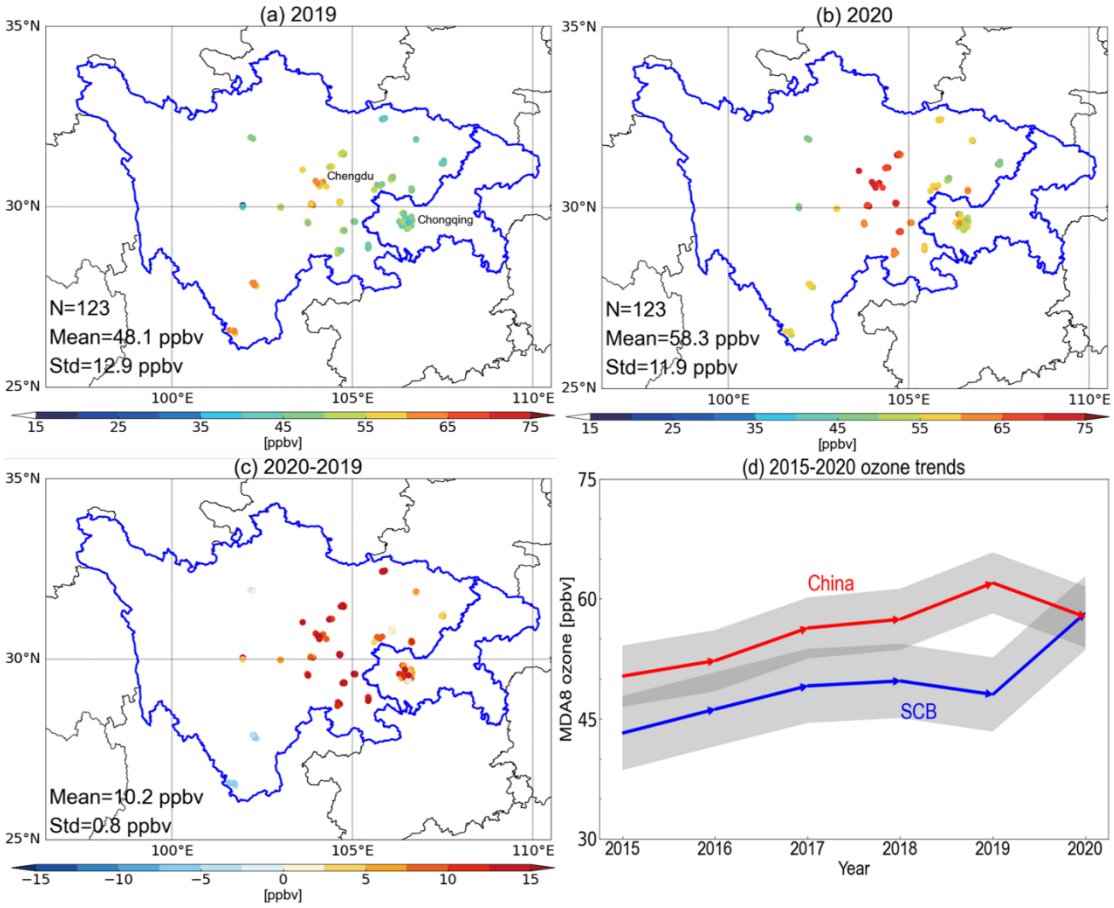

Figure 1 Surface O_3 enhancements over the SCB region in May-June 2020 vs. 2019. (a) Spatial distributions of May-June mean O_3 concentrations over the SCB region in 2019. Number (N) denotes available measurement sites for this year. We average the O_3 concentrations at all measurement sites in each city to form a city representative O_3 dataset. (b) Same as (a) but for 2020. (c) Differences between 2020 and 2019. (d) Trends in May-June mean ozone concentrations from 2015-2020 averaged for all Chinese cities (red) and for the SCB cities cluster (blue). Grey shadings represent the range of mean value ± 1σ STD across all cities. The base map of the figure is created by the Basemap package of Python.

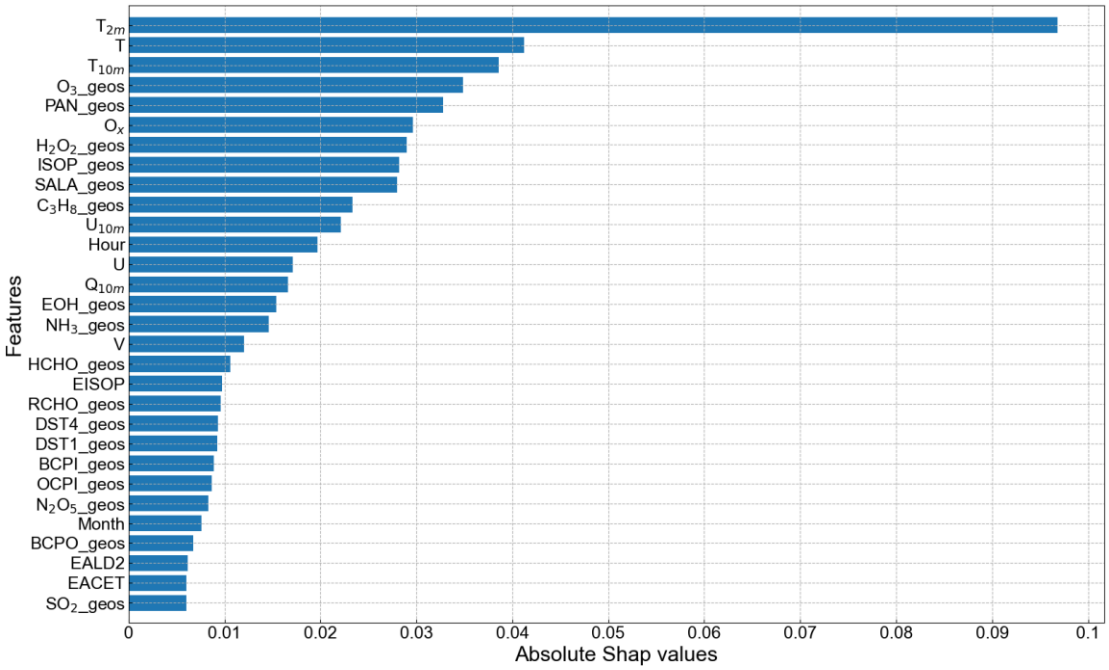

Figure 2 Importance of input variables for the XGBoost model trained to correct the GEOS-Chem model-to-measurement O_3 discrepancy over the SCB. Shown are the distribution of the SHAP values for each variable averaged over all cities in the SCB, ranked by the average importance of each feature. Higher SHAP value indicates higher feature importance. Descriptions for all acronyms are listed in Table S1. For clarity, only the top 30 variables are shown. See Figure S6 for importance of all variables.

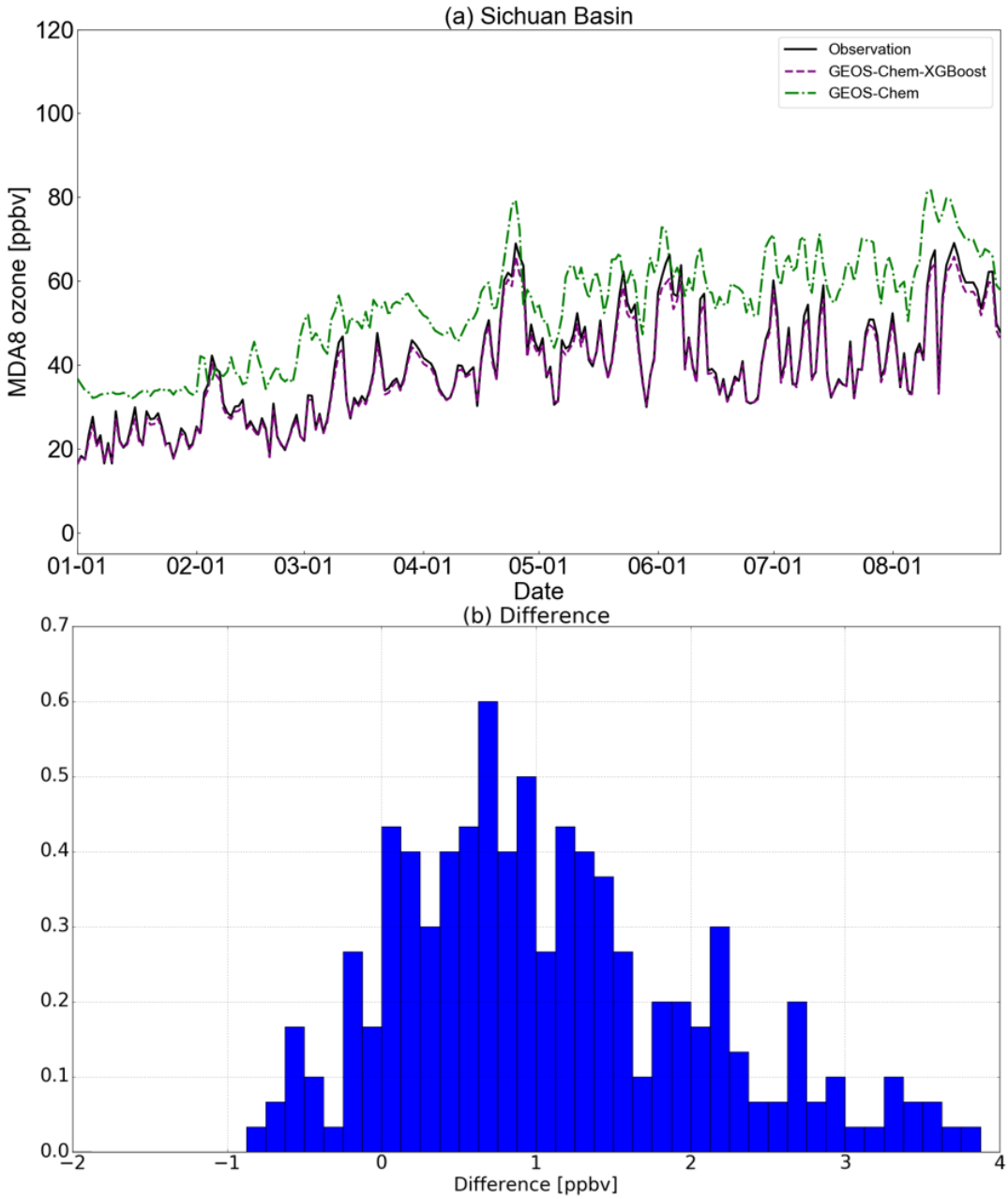

Figure 3 Measured and modelled O_3 variabilities over the SCB in 2019 (a). Measured, GEOS-Chem, and GEOS-Chem-XGBoost predicted O_3 values are denoted by black solid, grey dashed, and purple dashed lines, respectively. (b) Histogram of the differences between the GEOS-Chem-XGBoost predictions and the measurements.

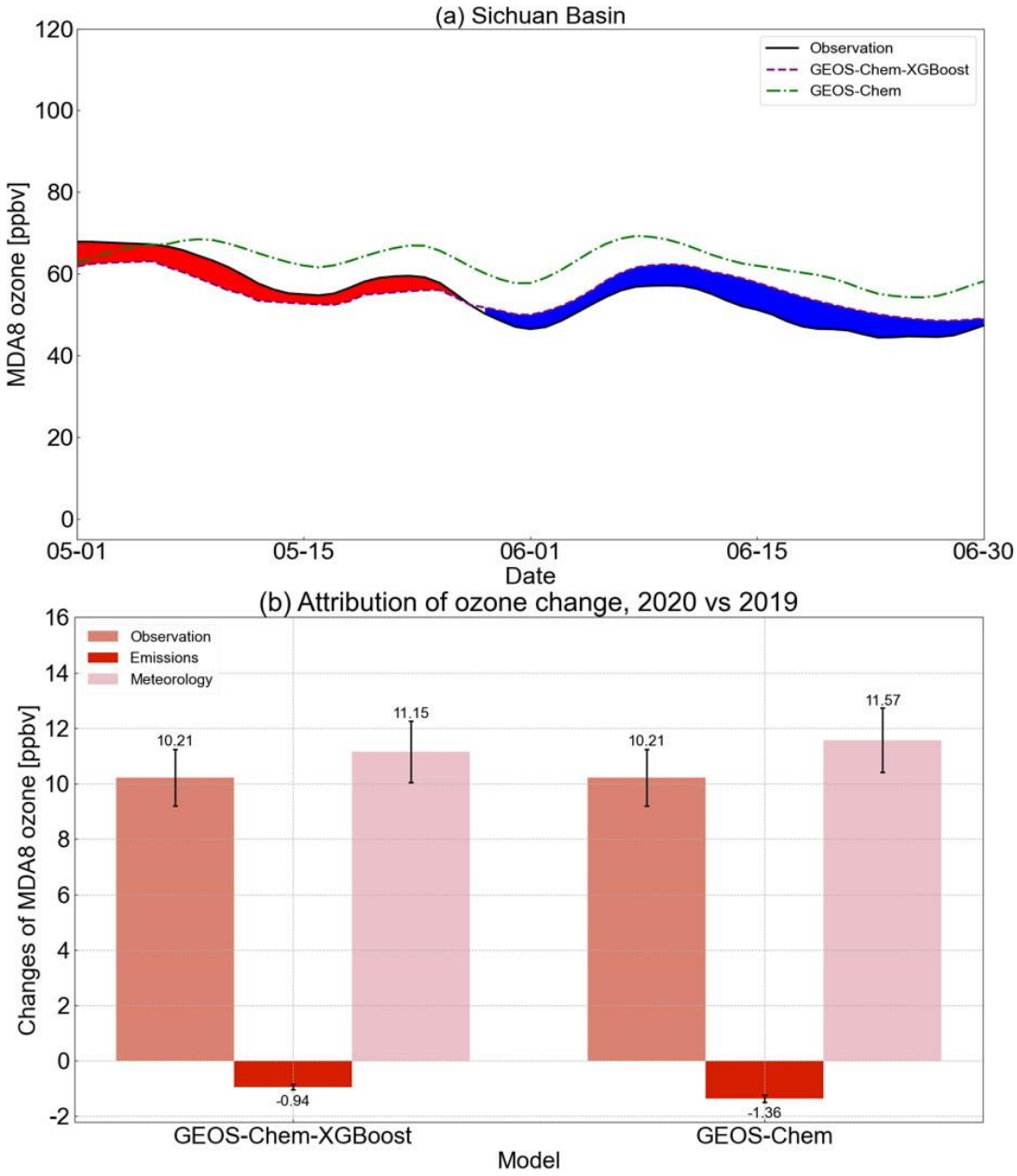

Figure 4 (a) Comparison of the GEOS-Chem-XGBoost O_3 predictions to the 2020 measurements. Red (blue) shadings represent where GEOS-Chem-XGBoost predictions are higher (lower) than the actual measurements in 2020, indicating that changes in anthropogenic emission lead to O_3 increase (decrease) in 2020. All values shown are 7-day average for presentation purpose. (b) Attribution of surface O_3 enhancements over the SCB in May-June 2020 vs. 2019. Filled colored bars denote O_3 change as seen from measurements, and due to changes in anthropogenic emission and meteorological conditions estimated by the GEOS-Chem-XGBoost model and the GEOS-Chem model. Black vertical bars represent 1σ STD across cities.

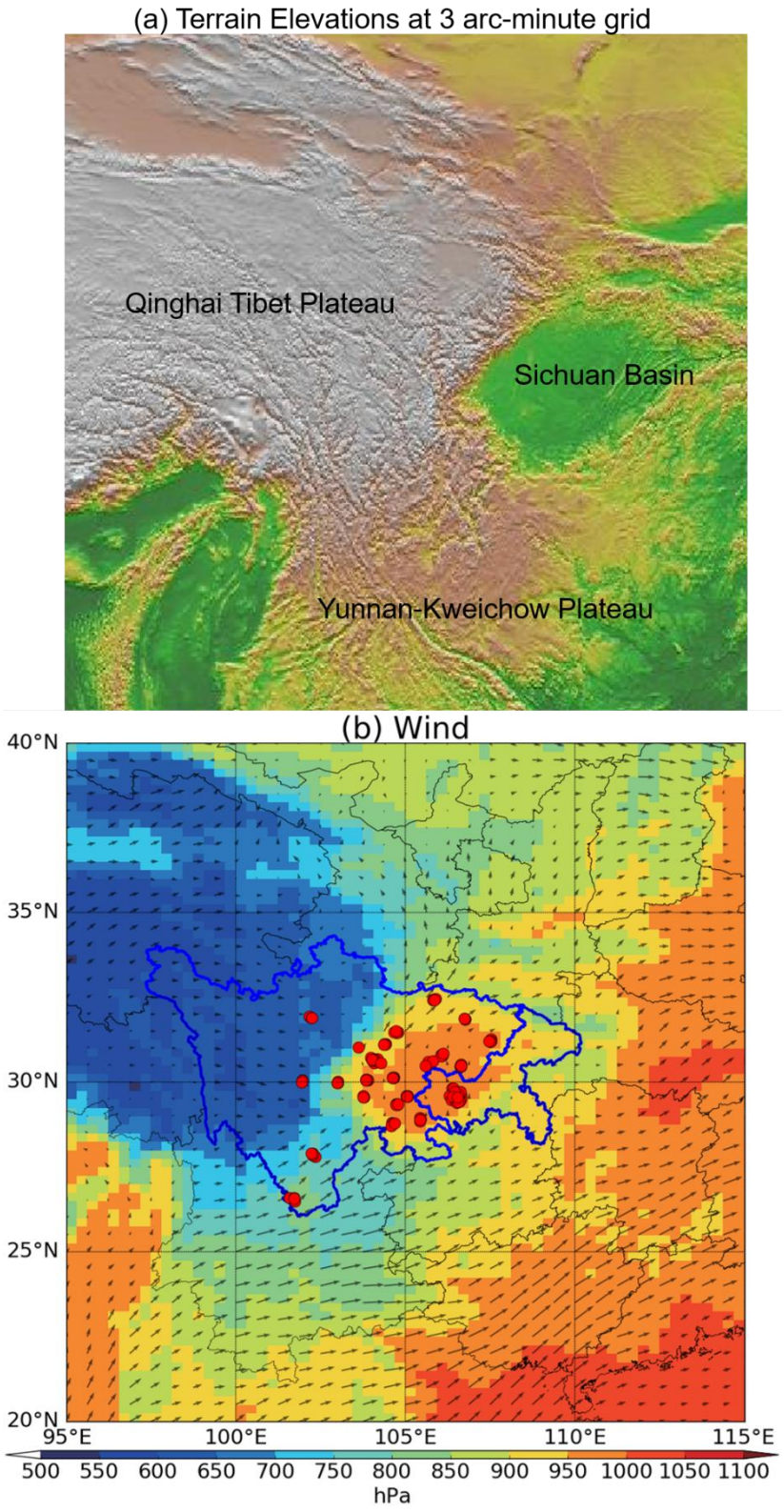

Figure 5 Terrain elevations (a) and surface temperature and wind fields (b) over the SCB and surrounding regions. The spatial resolutions for (a) and (b) are 3 × 3 arc-minute and 0.25° × 0.25°, respectively. The white area in black line is Tibetan Plateau (with altitudes of 4–5 km a.s.l.), the yellow area in red line is the Yunnan-Kweichou Plateau (2–3 km a.s.l), the green area in circle is the SCB (0.5–1 km a.s.l). The base map of the figure is created by the Basemap package of Python.

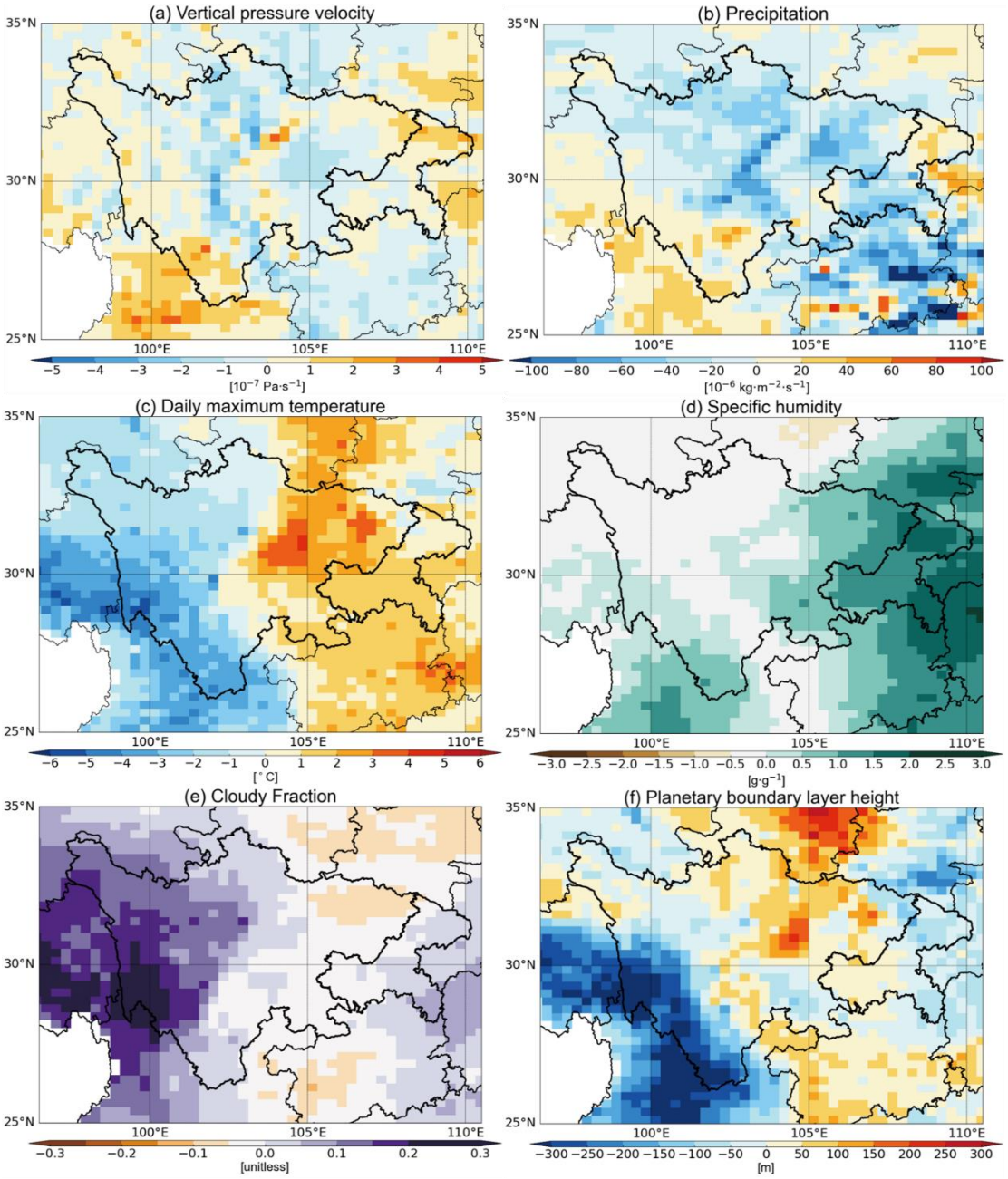

Figure 6 May-June mean differences in vertical pressure velocity (a), precipitation (b), temperature (c), specific humidity (d), cloud fraction (e), and PBLH (f) between 2020 and 2019 over the SCB and surrounding regions. All these meteorological parameters are from the GEOS-FP dataset. The vertical pressure velocity is prescribed at the PBLH and others are at the surface. The base map of the figure is created by the Basemap package of Python.

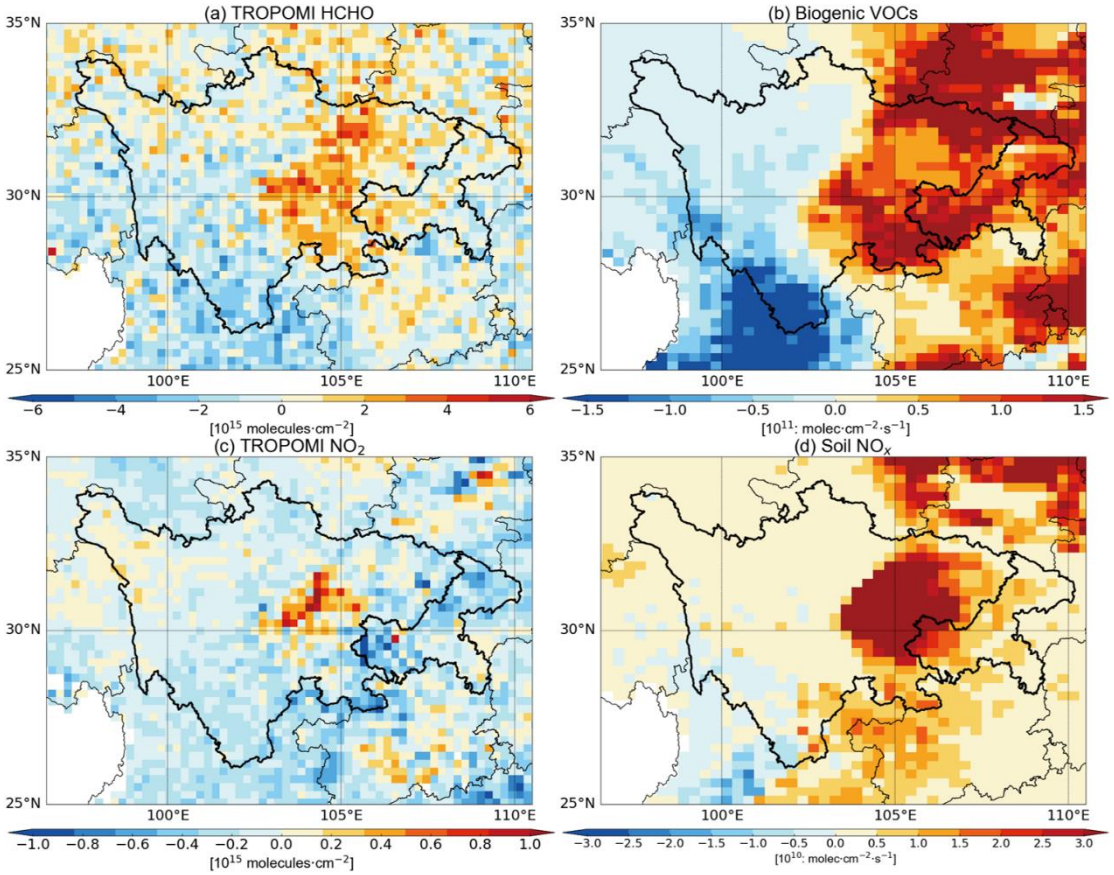

Figure 7 May-June mean differences in O_3 precursors between 2020 and 2019. (a) TROPOMI observed HCHO, (b) biogenic VOCs, (c) TROPOMI observed NO_2, and (d) Soil NO_x. Biogenic VOCs and soil NO_x are available from GEOS-Chem model online calculations. The base map of the figure is created by the Basemap package of Python.

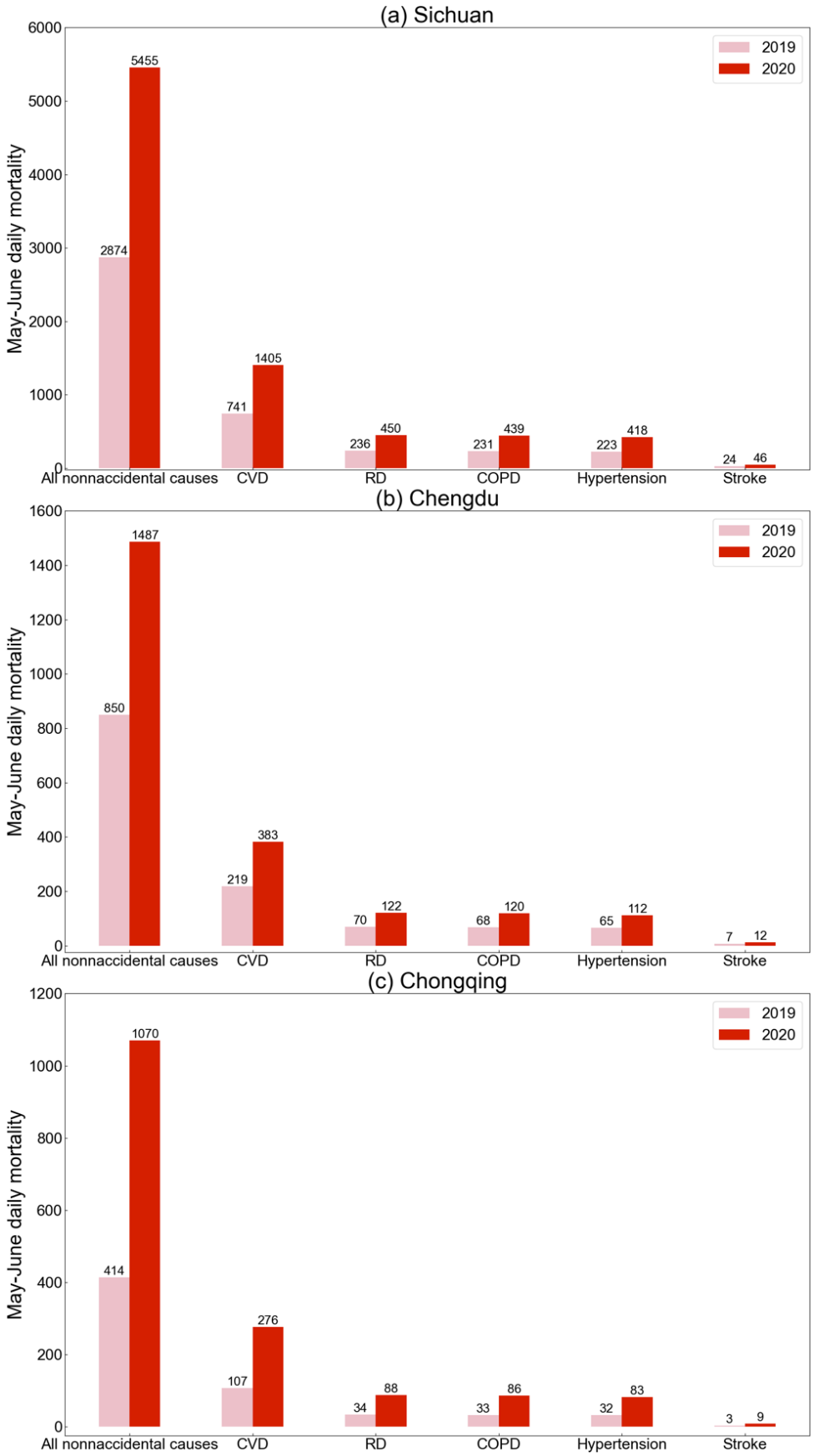

Figure 8 Total daily mortality from all non-accidental causes, CVD, RD, COPD, hypertension, and stroke attributable to ambient O_3 exposure over the SCB during May-June in 2019 and 2020.